The effect of surface charge on threshold flux and fouling behavior of silicon carbide membrane with O/W emulsion and sodium alginate solution as typical pollutants

TU Delft
Delft University of Technology

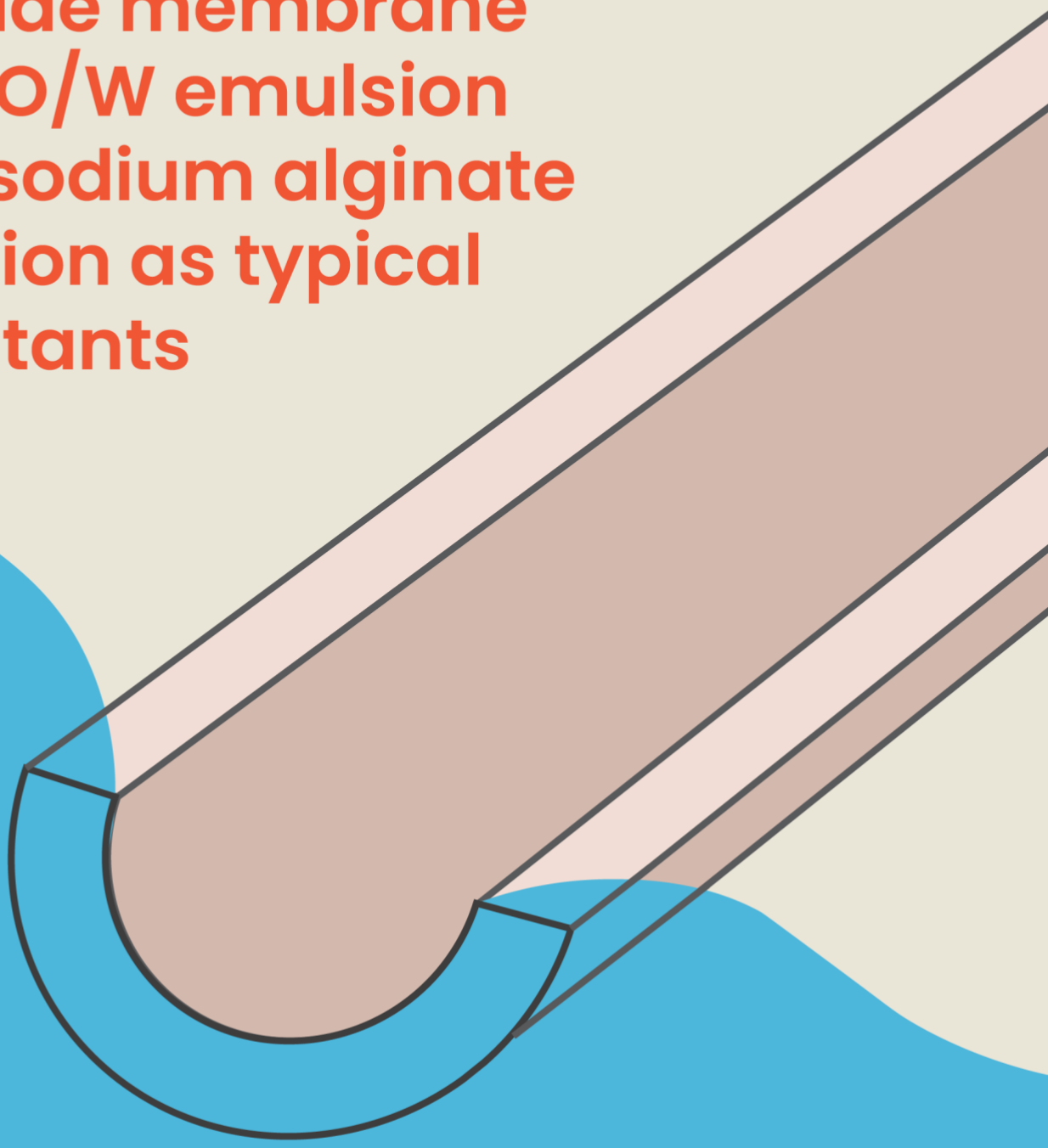

Guangze Qin

Title: The effect of surface charge on threshold flux and fouling behavior of silicon carbide membrane with O/W emulsion and sodium alginate solution as typical pollutants

by

Guangze Qin

August 2021

in partial fulfillment of the requirements for the degree of

Master of science

In applied earth science

Supervisors: Prof. dr.ir L.C. (Luuk) Rietveld
Assoc.Prof.dr.ir Bas Heijman
Dr. Paolo Sberna
Ir. Mingliang Chen

Abbreviations

C_f: concentration in feed solution (mgL^{-1})
C_p: concentration in permeate solution (mgL^{-1})
CVD: Chemical Vapor Deposition
CMC: Critical micelle concentration
COD: Chemical Oxygen Demand
O/W emulsion: oil and water emulsion
TMP: Trans-membrane pressure (bar)
TMP_{avg}: Average transmembrane pressure (bar)
SA: Sodium alginate
SDS: Sodium dodecyl sulfate
UF: Ultrafiltration
MF: Microfiltration
TOC: Total organic carbon
EPS: Extracellular polymeric substance
LPCVD: Low pressure chemical vapor deposition
PSD: Particle size distribution

ABSTRACT

Colloidal fouling has attracted increasing interest in the membrane field. Oil and water (O/W) emulsion droplet and Extracellular polymeric substance (EPS) are significant colloids in produced water and surface water, respectively. Oily wastewater is produced in many industrial processes such as oil and gas extraction processes, and can take a product, a by-product or a waste stream. In this study, silicon carbide (SiC) membranes were employed to separate oil droplets from O/W emulsion. The effect of ionic strength, pH, surfactant concentration on threshold flux of commercially SiC MF using O/W emulsion stabilized by the sodium dodecyl sulfonate (SDS) were investigated. The results indicated that the threshold fluxes, determined by both the TMP_{avg} method and fouling rate method, increased with an increase of SDS concentration, but decreased with the salinity when using commercial SiC MF membrane filtering 400 mg/L O/W emulsions. Besides, a higher threshold flux was observed for emulsions with a higher pH. Moreover, the high absolute value of zeta potential of O/W emulsion could alleviate fouling.

In the end, we produced SiC UF membrane by depositing SiC layer on the alumina supports by low pressure vapor deposition (LPCVD) due to its low fabrication cost. We investigated the anti-fouling abilities of pristine Al_2O_3 UF membrane and SiC-UF membrane by using sodium alginate as foulant (SA) solution in multi-stage experiments. When fouling experiments operated with pure SA solution or SA solution with a low calcium ion concentration, SiC UF membrane has a better anti-fouling ability compared with pristine Al_2O_3 UF membrane due to a lower reversible and irreversible fouling resistance and a slower increase of TMP.

ACKNOWLEDGEMENT

The two years in Delft were fleeting, and I finally ushered in the great moment of graduation. During this period, there were both laughter and tears. With gratitude, I want to finish my graduation thesis through my appreciation of the teachers, classmates, friends, and family who helped me. Firstly, I would like to express my most sincere thanks to my mentor Bas, who brought me to the exciting world of SiC membrane and inspired me when I was sad. Secondly, I would like to thank my daily supervisor Mingliang, who taught me how to use experimental equipment and how to test samples and gave me some theoretical guidance. Thirdly, I would also like to thank Professor Luuk for his valuable comments on the design of the experiment and the revision of the thesis. Moreover, I would also like to express my gratitude to my friends in my laboratory, including Shan, Jianyi, Feiyang, Zhouyuan, Connie, for your company to make the initially boring experiment enjoyable. I would also like to thank my sisters who traveled to Stockholm together during the Christmas holidays, including Xingyu, Xiaonan, Zixi, Jinnan, and the days with them are precious, especially in the COVID-19 period. In the middle of the project, my computer broke down. At this time, Wang Qian, who majored in microelectronics, lent me her computer so that I could graduate successfully on time. Thank you, my brother Siyuan, for his help in study and life, especially when you helped me move my household items. A special thanks to Xingyu because she helped me design the cover and gave me a lot of help and encouragement throughout the course of the graduation project. Finally, I would like to express my gratitude to my parents for their financial support. It is the biggest motivation for me to move forward. This graduation thesis is my starting point in the field of SiC membranes.

The two years in Delft have been the best two years in my life. In the past two years, I have accumulated a lot of professional knowledge, and at the same time, my academic literacy has been greatly improved. I feel fortunate to be able to continue my PhD under the guidance of Bas, and I hope that in the next four years of Ph.D., I can make more excellent academic progress and innovative results from this starting point and become who I want to be.

Guangze Qin,
August 19, 2021
Delft

CONTENTS

List of Figures

List of Tables

1. Introduction

1.1 Background and research problem statement

In the past decades, due to a rapid increase in population, increased industrialization, and agricultural needs, the consumption rate of water increased tremendously, which lead to water scarcity. Therefore, it is urgent to develop energy-efficient water treatment technologies with high surface-area-per-unit volume (Lee et al., 2015). The application of membrane technology in wastewater treatment has grown rapidly in recent decades due to its smaller footprint and higher removal efficiency compared with conventional water treatment technologies (Hofs et al., 2011).

According to pore sizes, membranes can also be classified into microfiltration (MF), ultrafiltration (UF), nanofiltration (NF), and reverse osmosis (RO) membranes. Based on the materials, membranes can be roughly divided into polymeric membranes and ceramic membranes. Polymeric membranes are dominant in the membranes market so that they were intensively reported in terms of membrane modifications, membrane applications, membrane fouling issues, and membrane cleaning. However, due to stronger mechanical strength, excellent thermal conductivity, high water permeability, and outstanding chemical stability compared with polymeric membrane, the ceramic membrane has attracted increasing attention in academia and industry (Sholl et al., 2016). Silicon carbide (SiC) ceramic membrane has advantages compared with other ceramic membranes, such as higher hydrophilicity and lower fouling tendency. Therefore, the application of SiC ceramic membranes is conducive to solve the problems of serious scaling of conventional alumina ceramic membranes and poor thermal and chemical stability of organic membranes, and then plays an important role in the treatment of corrosive industrial wastewater (Chen et al., 2020). However, currently only SiC UF membranes are commercially available. The formation of Si-C needs a high sintering temperature. As a result, SiC UF membranes are expensive. Using SiC as a deposition material in the pores of alumina (Al_2O_3) under a relatively lower temperature by low pressure vapor deposition (LPCVD) can be a good way to decrease the fabrication cost for facilitating the application of ceramic membrane (Chen, 2020).

Colloidal fouling has attracted increasing interest in the membrane field. O/W emulsion droplet and Extracellular polymeric substance (EPS) are critical colloidal in produced water and surface water, respectively. Oily wastewater is generated in a variety of industrial processes, including oil and gas extraction, and can exist as a product, a by-product, or a waste stream. Membrane filtration, especially for UF membrane filtration, is a cost-effective and selective way of separating water from the oil of O/W emulsion. This is especially the case for stable emulsion with droplet sizes smaller than 10 μm,

which could not be effectively separated by traditional methods such as flotation (Zouboulis et al., 2000). Besides, according to the definition of the critical flux, no change in resistance with time is permitted at fluxes less than either form of the critical flux (Field & Pearce, 2011). The concept of critical flux is essential but does not give helpful guidance in a practical situation and could not provide a precise suggestion for the operator in the membrane-related industry (Field & Pearce, 2011). Therefore, a more realistic concept is recommended which is called 'threshold flux', and the threshold flux of commercial SiC MF has been determined in this study. In the real oily wastewater treatment process, different oily water has different pH and salinity. The threshold flux of organic membrane has been widely investigated (He et al., 2017; Kirschner et al., 2017). However, to the best of our knowledge, the threshold flux of commercial SiC MF membrane has not been studied yet. In this research, we investigated the effect of ionic strength, pH, surfactant concentration on threshold flux of 100 nm commercial SiC MF membrane produced by Liqtech company using an emulsion stabilized by the sodium dodecyl sulfonate (SDS).

In the end, in the aspect of treating surface water, the antifouling ability of pristine Al_2O_3 UF membrane and SiC UF membrane is unknown. Sodium alginate (SA) has been chosen as a model foulant since it is commonly used as a substitute for EPS, which is the main organic pollutant in surface water (Katsoufidou et al., 2017). For SA filtration, the effect of calcium ions and ion strength on membrane performances and fouling mechanisms of SiC UF membrane and Al_2O_3 UF membrane are not clarified. Therefore, we performed constant flow filtration experiments at dead end mode using SA solution with different calcium concentrations and salinity. By comparison, the reversible/irreversible fouling resistance, and the rejection rate of SA under the above conditions could be calculated. Besides, the effect of calcium ions and ion strength on membrane performances, and fouling mechanisms of SiC UF membrane and Al_2O_3 UF membrane could be explained.

1.2 Research Question

A growing number of publications focus on the threshold flux of organic membranes or ceramic membranes such as Al_2O_3 membranes (He et al., 2017; Kirschner et al., 2017). To the best of our knowledge, the threshold flux of commercial SiC MF membrane has not been reported in the literature. The first objective is to determine the threshold flux of SiC MF membrane using O/W emulsions as model foulant.

Besides, most published papers are based on one-stage experiments when filtering SA using UF and NF membrane (Li et al., 2014; Katsoufidou et al., 2017). Pure SA solution or SA solution with different calcium concentrations and salinity have not been tested before with SiC UF membranes produced by LPCVD in multi-stage experiments. The second objective is to assess the performance of SiC UF membranes and Al_2O_3 UF

membranes using SA solution as a model foulant in multi-stage experiments and calculate the fouling resistance of membrane and obtain the retention of SA. The purpose is to answer the following questions.

1. What is the influence of calcium ions and ion strength on membrane performances and fouling mechanisms of SiC UF membrane?

2. Which type of membrane (pristine Al_2O_3 UF membrane or SiC UF membrane) has better anti-fouling ability when using SA solution as model foulant?

3. What is the threshold flux of commercial SiC MF membrane when filtering different O/W emulsions with different pH, salinity, SDS concentration (400 mg/L O/W emulsion with 100 mg/L SDS, 400 mg/L SDS, 800 mg/L SDS, pH = 3, pH = 8, 10 mmol/L NaCl, 100 mmol/L NaCl)?

4. What is the effect of SDS concentration, salinity, pH on the zeta potential of O/W emulsions and fouling phenomenon of commercial SiC MF membrane?

1.3 Thesis structure

To solve the above research questions, literature review and laboratory research can be applied to draw hypotheses and results. And this thesis could be separated into seven chapters.

Chapter 1: Introduction

Chapter 1 illustrated the background information, knowledge gap of this research and the relevant research questions.

Chapter 2: Literature review

The literature presented in Chapter 2 illustrated the properties and application, characterization of SiC membrane and two types of model foulants, followed by a comparison of the threshold flux and critical flux, and in the end, the main fouling mechanism of SiC ceramic membrane has been identified.

Chapter 3: Material and Methodology

When the research started, the experimental data (TMP, COD, TOC, etc.) were measured. Drawing the figure and explaining the tendency based on the theories illustrated in Chapter 2 by using calculated results. To effectively answer the research questions, laboratory experiments such as pure water flux test and filtration test were conducted to collect the TMP with filtering time and frequency.

Chapter 4: Results and discussion

This chapter shows the data of experiments and plot figures, finding the possible explanation behind them.

Chapter 5: Conclusion

This chapter answers the research questions and concludes the main findings in the study.

Chapter 6: Limitations and recommendations

Chapter 6 shows the limitations of the current study in the aspects of experiment facilities and the design of the experiment. This chapter also provides advice for future research.

2. Literature review

2.1 The properties and application of SiC membrane

Ceramic membranes have gained popularity because they have outstanding resistance to mechanical, chemical, and thermal treatments and show high porosity and a uniform pore size distribution. Currently, mass-produced inorganic membranes are mainly made of Al_2O_3, ZrO_2, TiO_2, Si, or ZnO. Among these, Al_2O_3 is the most common membrane. Compared to alumina, SiC membranes show a higher corrosion resistance to strong acid and alkaline environments, have an excellent thermal shock resistance up to 800 ^oC, higher permeate flux, higher negatively charged surface, and higher hydrophilicity (Shin et al., 2010). Especially, SiC ceramics show super hydrophilic properties and increased permeability in the filtration of water. Y.J.Shin reported that the contact angle of water on SiC substrates is 70^o (Shin et al., 2010). It is known that the contact angle of hydroxyl groups exhibit is zero. The contact angle of the SiC membrane is close to 0^o duo to the hydrophilic hydroxyl groups of the SiO_2 layers that are formed on the SiC surface. Moreover, SiC exhibits considerably lower fouling properties as compared to other ceramic membranes due to its low isoelectric point, which is around 2.6 (Hofs et al., 2011). The fouling behavior of a membrane can be determined by measuring, at constant flux, the increase in TMP as a function of time (Lee et al., 2015). Results of membrane fouling by direct filtration of lake water are depicted in Fig. 1, which shows the lowest fouling for SiC.

Similarly, the treatment of produced water by using different organic and inorganic membranes has been investigated. The results show that SiC membranes have lower reversible and irreversible fouling and higher chemical and thermal stability compared with membranes made of polyvinylidene fluoride (PVDF), and ZrO_2 (Eray et al., 2021). Therefore, SiC membrane can be efficiently cleaned at high temperatures and in a wide pH range. And SiC MF membrane with pore size 100 nm from Liqtech has been used to treat olive mill wastewaters, showing high efficiency of removing chemical oxygen demand (COD) and suspended solids (Eray et al., 2021).

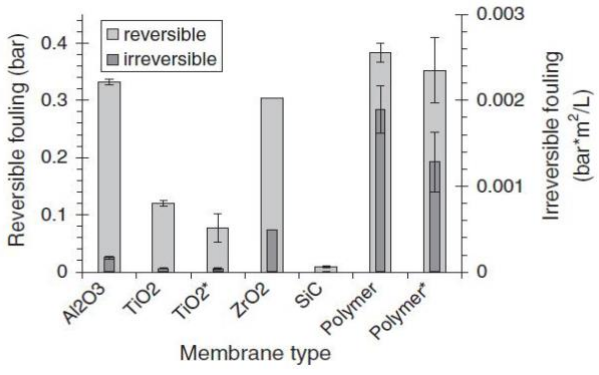

Fig. 1. TMP increases due to reversible and irreversible fouling for different membrane materials (Hofs et al., 2011).

The fabrication of SiC membrane can be achieved by three steps: (a) Preparation of ceramic power suspension (b) shaping of ceramic suspension (c) heat treatment including calcination and sintering (Li, 2007). After the above steps, additional layer deposition steps such as sol-gel methods, Chemical Vapor Deposition (CVD), and Atomic Layer Deposition (ALD) can narrow the pore size of the membrane and improve membrane selectivity. Till now, SiC thin layer technology is mainly performed by CVD in which one or more volatile precursors diluted with reactive gasses are applied simultaneously in a continuous flow in a heated reactor with vacuum environment. In this way, layer thicknesses of 10 nm and more are applied in the pores and on top of a macroporous substrate (Uhlhorn et al., 1992). Chen et al. reported that LPCVD, using SiH_2Cl_2 and C_2H_2 as precursor gasses, is a good way for the deposition of SiC on the alumina membrane support since the interactions with pollutions mainly happens at the selective layer surface (Chen et al., 2020). However, for nanofiltration membranes, having pores less than 1 nm, the CVD layer is too thick, resulting in plugging of the pores. To be able to tune the pores in SiC nanofiltration membranes precisely, ALD-technology might offer a better solution compared with the commonly used sol-gel method (Chen et al., 2017). In literature, details can be found on the mechanisms of SiC layer growth on a wafer by the alternate supply of SiH_2Cl_2 and C_2H_2 (Maaskant et al., 2018). However, a combination of ALD with SiC coating techniques for membrane preparation has not been investigated yet.

Currently, it is reported that only SiC UF membranes with pore sizes of around 200 nm are commercially available. Several previous studies reported current SiC nanofiltration membranes to show low fluxes and low retentions. For example, König et al. reported that the fabrication of a defect-free SiC layer on a 200 nm SiC support is using an easy one-step dip coating of a suspension containing a polymer, followed by partial pyrolysis of this (preceramic) polymer (König et al., 2014). In this way, a selective layer was obtained with pores smaller than 5 nm and low water permeation, which is around 0.06 $L\ m^{-2}\ h^{-1}\ bar^{-1}$. On the other hand, a host of studies that focus on the development of SiC gas separation membranes, prepared via partly pyrolysis of a preceramic polymer resulting in a nanoporous structure.

Many parameters like polymer choice, crosslinking of the polymer, heat treatment, and the type of sintering additives play a critical role in the morphology formation of the material. An example is a SiC gas separation membrane, developed by Suda et al., with pores between 0.6-0.8 nm depending on the way the preceramic polymer was crosslinked (Suda et al., 2006; König et al., 2014). Next to this, Atomic Layer Deposition (ALD) is described as an interesting potential route for the fabrication and modification of ceramic membranes (George et al., 2010; Song et al., 2016). Shang et

al. firstly illustrate the fabrication of tight TiO_2 NF membranes (pore sizes of about 0.5 nm and a molecular weight cut-off (MWCO) of 300 Da) by using ALD. After modification, the membrane maintains a relatively high permeability, which is greater than that of the commercially available tight polymer NF membrane (Song et al., 2016). ALD was used to provide a coating of metallic oxides layers in porous materials such as (micro) pore walls and catalysts. Also, TiO_2 NF membranes were made via atomic layer deposition by Chen et al. (Shang et al., 2017). Here, on tubular α-alumina support, a TiO_2 layer was applied by sol-gel techniques, resulting in a membrane with pores of 5 nm. The pores of this layer were modified with atomic layer deposition, and with increasing ALD cycles, decreasing pore size was observed. After 200 ALD cycles, an MWCO of ~2600 Da and a water permeability of 45 L m^{-2} h^{-1} bar^{-1} were measured, and after 300 ALD cycles, an MWCO of ~680 Da and a water permeability 30 L m^{-2} h^{-1} bar^{-1} were measured, which is higher than many conventional tubular NF membranes prepared via the sol-gel process. This research shows that ALD is an effective measure to reduce the pore size of the ceramic membrane, regarded as a new way to fabricate and modify nanofiltration ceramic membrane with high permeability.

Both surface hydrophilic and charge of the surface group plays a vital role in the severity of membrane fouling. A lower negative zeta potential could bring a lower electrostatic repulsion between the foulant and the membrane. SiC-alumina UF membranes are mainly made of metal oxides such as silica and alumina, which means the surface of the membrane is rich in hydroxyl groups, which easily form hydrogen bonds with water, giving it a high hydrophilic characteristic. Therefore, nearly all SiC membranes are naturally hydrophilic (Kujawa, J., & Kujawski, W, 2016). Moreover, with the increase of pure water flux, the hydraulic resistance of the fouling layer also increases with increasing permeation rate, resulting in the increase of irreversible fouling (Hong and Elimelech, 1997). Besides, membrane permeability is influenced by the hydrophilicity of the membrane with evaluating water contact angle. The higher the water contact angle, the lower the hydrophilicity will be, resulting in lower water permeability. Fraga reported that the range of water contact angle of SiC is 14°– 22° (Fraga et al., 2017), which will become as low as zero after oxidation. Williams et al. have similar findings, reporting that the water contact angle for SiO_2 over the surface of the membrane approaches zero. But they also found that with the decrease of the thickness of the oxides layer, the hydrophilic increases (Williams et al., 1974). Therefore, a thicker oxidized SiC surface could offer improved water permeability and hydrophilicity.

Membrane permeability and fouling resistance are closely linked to the surface chemical properties of the material. Pure SiC particles surface can oxidize to SiO_2 when exposure air at room temperature. (Soukiassian et al., 2005). Therefore, a thin oxide layer exists over the SiC particle surface is a common phenomenon for SiC membranes (Roy et al., 2014). Due to its low isoelectric point (pH = 2.5), SiC has excellent

antifouling properties (Zhang et al., 2017). When SiC is oxidized to SiO_2, the surface isoelectric point will become even lower (pH = 2.2) (Gun'Ko et al., 1999). Therefore, improving the membrane surface properties can be achieved by an oxidation-bonding approach. However, due to the covalent nature of Si-C, the production of SiC ceramic membrane requires a higher sintering temperature. But with the increase of sintering temperature, the amount of amorphous SiO_2 will increase, which decreases the chemical stability of the membrane and the idea sintering temperature is 800-1000^{o}C (Bukhari et al., 2018).

2.2 Membrane fouling

2.2.1 Factors influencing fouling

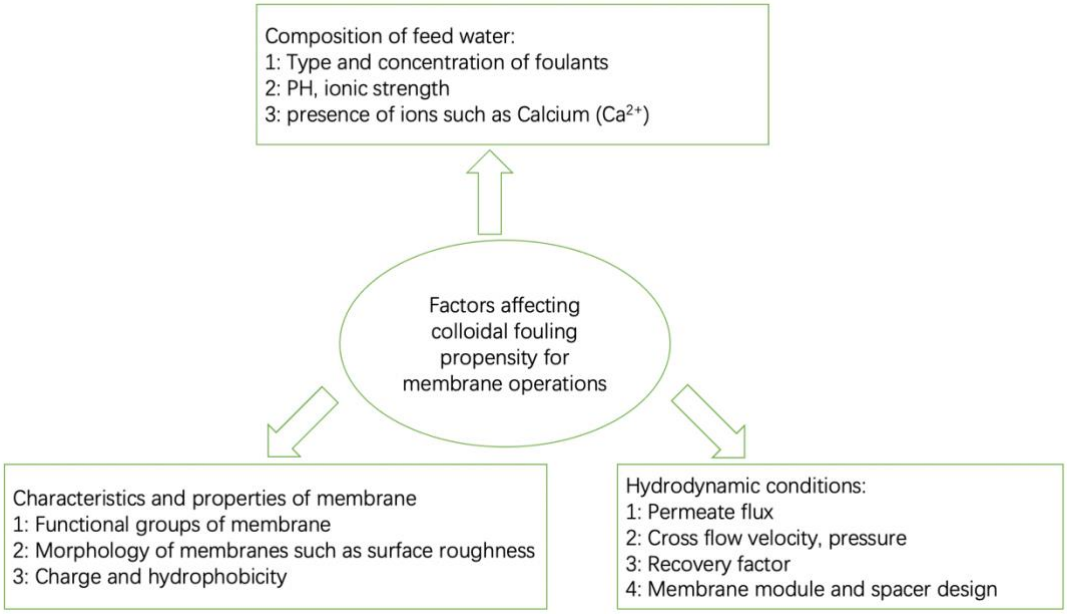

Fig. 2. Factors influencing membrane fouling (adapted from Tang et al., 2011).

Colloidal fouling is a complicated problem. As shown in Fig.2, factors influencing fouling can be divided into three groups: composition of feed water, membrane characteristics, and operational conditions (Tang et al., 2011).

The first group is a composition of feed water. The concentration and physiochemical properties (charge, size, functional group) strongly influencing the fouling phenomenon (Buffle et al., 1998). For instance, the colloidal surface charge is a significant function of the pH and ionic strength of the solution (Hong & Elimelech, 1997). Therefore, solution chemistry parameters (pH, ionic strength, and composition) are the main contributing factors in colloidal fouling. Lee et al. reported that electrostatic interactions between the EPS or alginate molecules play a vital role (Lee et al., 2006). With decreased pH or increased ionic strength, gel formation is promoted, and thus membrane fouling can be alleviated by gel formation. The reason is that the double-

layer compression and charge screening reduce the charge of the macromolecules, resulting in the reduction of the electrostatic repulsion between the macromolecules, thereby promoting the deposition and accumulation on the surface of the membrane (Lee et al., 2006; Lee & Elimelech, 2007).

The pH value affects the charge of the solute and the charge of the membrane (Verliefde et al., 2007a), thus affecting the rejection rate of foulants. Lobo et al. found that the membrane became positively charged at low pH (pH = 3), adsorbing the anionic surfactant from the emulsion and increasing the hydrophobicity of the membrane surface, which allows surfactant molecules to pass through the membrane and also resulting in a decrease in flux (Lobo et al., 2006). Besides, the rejection rate of negatively charged ions increased with a pH of feed lower than the isoelectric point of the membrane due to increased electrostatic repulsion between negatively charged membrane surface and negatively charged ions (Verliefde et al., 2009c). Therefore, lowering pH by adding acid is another way to reduce fouling.

The second group is membrane properties. The membrane fouling is affected by membrane properties, including pore size distribution, charge and density of surface group, surface hydrophilicity. Firstly, during filtration experiments using O/W emulsion stabilized by SDS, negatively charged and more hydrophilic membranes tend to show better anti-fouling abilities at the initial stage of membrane fouling. Besides, during SA filtration, membranes with larger pores are susceptible to internal fouling, but membrane with smaller pore size shows greater initial fouling (Ye et al., 2015). Moreover, compared with polymeric membranes, the ceramic membranes, which are generally made of metal oxides that are more hydrophilic than most polymeric materials, had a smaller absolute value of zeta potential, much less negative surface charges, and lower contact angle. Membrane hydrophobicity had a positive correlation with static contact angle, ceramic membranes have a smaller static contact angle, so ceramic membranes were much more hydrophilic than polymeric membranes (Lee et al., 2014). It is reported that irreversible fouling could be reduced when the charge of the stabilization surfactant of oil/water emulsions is opposite to the membrane (Nagasawa et al., 2020). When the membrane and the oil droplets have the same charge, the electrostatic repulsion will prevent the oil droplets from penetrating into the pores, but the electrostatic repulsion will also inhibit the deformation of the oil droplets so that the oil droplets will sink into the pores and the membrane's pore size will be narrowed, thereby causing decreasing of water flux. When the membrane and the oil droplets have opposite charges, the oil droplets will deform and enter the pores. Although the water flux is high, the oil concentration in the permeate will be high (Nagasawa et al., 2020).

The third group is operational conditions. Hydrodynamic conditions, such as permeate flux and cross flow velocity (CFV), have a significant effect on membrane fouling. Specifically, severe fouling may develop with a high membrane flux and a low

crossflow. The higher CFV resulted in a larger Re. Theoretically, turbulent flow is defined as Re exceeding 4000 (Hua et al., 2007). Therefore, higher CFV create turbulence since turbulent flow can overcome concentration-polarization (Wang et al., 2011).

2.2.2 Fouling mechanism

The fouling mechanism for MF membrane fouling can be explained by three stages (Zhu et al., 2017). The first stage is the accumulation of oil droplet on the membrane surface, followed by the formation of the cake layer, in this stage, the interaction between oil droplets dominates. The second stage is droplet form due to the pressure drop across the cake layer. The third stage is the oil droplet spread along the membrane surface, which is also called membrane wetting. It can be explained that during fouling experiments, the formation of cake layer resulted in the linear increase in pressure observed in the first stage, which is linked with a cake layer that is incompressible. However, once the pressure drop across the cake layer reaches a critical value, which is determined by the characteristics of emulsion and membrane such as droplet size, and interfacial tension of droplet, resulting in exponential fouling in the MF process. The start of membrane wetting can be distinguished by irreversible membrane fouling. At the same time, oil drop deformation occurs. When operating below the flux where the pressure drop across the cake layer reaches a critical flux, hydraulic cleaning (backwashing or forward washing) can be used to restore the membrane flux. However, once the membranes become wetted by the oil, there is a limited effect in restoring flux by hydraulic cleaning, and chemical cleaning should be used. Also, when the oil drops on the bottom of the cake layer deform, there is an increase in contact area with the membrane surface, increasing the ability to wet the membrane. Overall, the dead-end and crossflow filtration experiments of the MF membrane show that there is a three-stage fouling mechanism: The first stage is the accumulation of oil droplet on the membrane surface, followed by the formation of cake layer, in this stage, the interaction between oil droplets dominates. The second stage is droplet form due to the pressure drop across the cake layer. The third stage is the oil droplet spread along the membrane surface (Ye et al., 2005; Ye et al., 2006).

2.2.3 Fouling mechanism in threshold flux determination

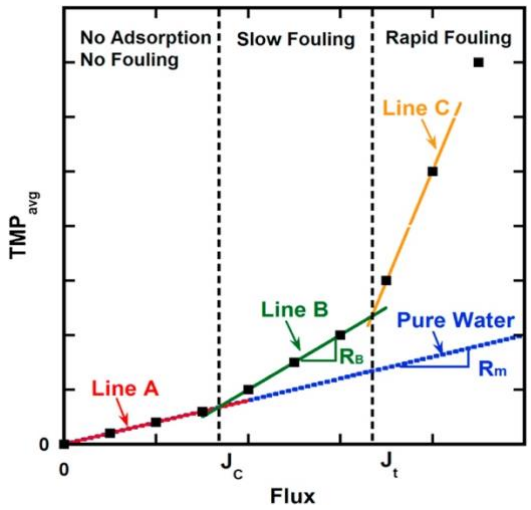

Fig. 3. An illustration of how to determine critical and threshold flux (He et al., 2017).

As shown in Fig.3, the dashed blue line represents the TMP-flux relationship corresponding in the absence of fouling which occurs during pure water filtration. In the first stage, red line (Line A) is the linear regression of TMP_{avg} below J_c, and the slope is related to clean membrane resistance. The green line (Line B) is the linear regression of TMP_{avg} between J_c and J_t, and slope means a constant resistance. The yellow line (Line C) represents the linear regression of the first two data points beyond J_t and is associated with exponential or rapid fouling.

2.3 Two types of the model solution

2.3.1 SA

Most foulants contributing to fouling are negatively charged. The model foulant SA ($NaC_6H_7O_6$) is a cell wall component of marine brown algae with a molecular weight of 12,000-800,000 g/mol and a diameter 6-20 nm (Nghiem et al., 2010). SA is commonly used as a substitute for EPS, which is the main organic pollutant in wastewater (Katsoufidou et al., 2017). Zhao et al. reported that alginate is commonly negatively charged in solution because it is rich in carboxylic and hydroxyl groups (Zhao et al., 2018). The carboxylic group plays a key role in the severity of irreversible fouling, and the hydroxyl group was a key factor dominating the reversible fouling (Bazin et al., 1995). Alginate fouling can be alleviated through physical cleaning by heating ceramic membrane in the oven and chemical cleaning by using NaOH, which are able to reduce the adhesion force between the organic foulants and the membrane surface (Li et al.,2014). After NaOH cleaning, ceramic membranes' zeta potential was more negative than pristine ones (Zhao et al., 2018). Besides, when alginate is attached to the surface of the membrane or into the membrane pore, the hydrophilicity and

negative charge of the membrane surface would increase (Simon et al., 2013), especially for SiC membranes with low surface charge density.

2.3.2 O/W emulsion

Oil/Water emulsion is another foulant that is also negatively charged by using negatively charged surfactants. And it can be stabilized by surfactants.

2.3.2.1 Treatment of O/W emulsion

Due to the rapid industrial development, a large amount of oily wastewater is produced in oil extraction, metallurgical, food, petrochemical and beverage industries. A challenge is how to treat the oily wastewater effectively and efficiently since the discharge of untreated oily wastewater will lead to serious contamination of groundwater, surface water and even be harmful to human health. Therefore, different regions published different discharge standards. For example, in the North Sea region, the amount of oil in the oily wastewater discharged should be below 30 mg L^{-1}, and the concentration of oil in domestic wastewater is typically between 50 and 400 mg L^{-1} (Daud et al., 2015). The oil concentration in produced water produced from the process of oil/gas extraction processes is typically between 3000 and 20,000 mg L^{-1}. Therefore, regardless of whether it is domestic wastewater generated by humans or industrial wastewater generated by the oil or petrochemical industries, further treatments are needed for oily wastewater recovery. Besides, the forms of oil in water can be roughly classified into three categories based on oil droplets diameter: free oil (>150 μm), dispersed oil (20-150 μm) and emulsified oil (< 20 μm) (Tanudjaja et al., 2017).

At present, the most commonly used water treatment technologies for treating oily wastewater include: (i) coagulation and dissolved-air flotation (Zouboulis et al., 2000), (ii) gravity-based separators (López-Vazquez et al., 2004), (iii) centrifugation (Cambiella et al., 2006) and (iv) hydrocyclone (Bai et al., 2011). The choice of oil-water separation methods depends on oil droplet size/ concentration and the chemical composition of feed water. However, if the oil content is low than 400 ppm and the majority of oil droplets are smaller than 20 μm, the processes mentioned above have a poor separation efficiency (Ahmad et al., 2020). However, the effectiveness of the separation process may be enhanced by increasing the size of the oil droplets through filtering by bed coalescence (Govedarica et al., 2015), but for turbid wastewaters, this method is hard to carry out. Another important problem that should be considered is that the composition is complex because they often contain a number of negatively charged surfactants (Kundu & Mishra, 2016), which impedes their treatment. Most importantly, the conventional methods cannot treat oily wastewater with oil droplet size below 20 μm. The solution for dealing with the problem mentioned above is the membrane-based oil and water separation techniques.

The UF has been confirmed as a predominant way to deal with oily water compared with organic membranes due to its hydrophilicity (Fakhru'l-Razi et al., 2009).

2.3.2 The influential factor on emulsion stability

As described in Derjaguin–Landau–Verwey–Overbeek (DLVO) theory, it is showed that colloidal stability is influenced by the potential energy of colloidal particle interactions under certain conditions (Israelachvili, 1972). The total potential energy is the sum of the van der Waals attractive potential energy plus the electrostatic repulsion potential energy produced by the electric double layer, as shown in equation 2.1. Johannes Diderik van der Waals attraction and electrostatic repulsion are the forces acting between these two potential energies. These two opposing forces determine the colloid's stability.

$$V_T = V_A + V_R \quad (2.1)$$

Where V_T is total potential energy, V_A is van der Waals attractive potential energy, V_R is the electrostatic repulsion potential energy.

Due to electron screening, the electrostatic repulsion between the oil droplets decreased and increased the tendency for deposition as a cake layer (Elzo et al., 1998). And less negatively charged oil droplet gives lower critical flux. The result of zeta potential shows that with an increase of salts concentration, the absolute value of zeta potential decreases, lower than 30 mV, which means the emulsion is not stable (Elzo et al., 1998).

The interfacial tension is reduced when the concentration of NaCl is increased in the presence of SDS, according to Dickhout et al. (Dickhout et al., 2019). By adding positively charged ions (Na^+), the negatively charged SDS head groups are screened. This reduces the electrostatic attraction between the head groups, allowing for the adsorption of more surfactant molecules. Additionally, the emulsion may become unstable due to the sodium ions screening the electrostatic repulsion between the droplets.

Apart from salinity, pH also influences the stability of the O/W emulsion. When pH is lower than the isoelectric point, the molecule or oil droplet is positively charged. The molecule or oil droplet has no net charge at the isoelectric point, whereas it is negatively charged at higher pH values (Dickhout et al., 2019). Therefore, to keep O/W emulsion stable, adjusting the pH of the aqueous phase far above or below the isoelectric point is essential.

2.4 Critical flux and threshold flux

2.4.1 Definition of critical flux and threshold flux

Field et al. (Field et al.,1995) first came up with the definition of critical flux. And he further illustrates the differences between the critical, threshold, and sustainable flux. According to the strict definitions of the strong and weak forms of the critical flux, no change in resistance with time is permitted at fluxes less than either form of the critical flux (Field & Pearce, 2011). As a result, the TMP must remain constant below the critical flux even while the membrane filters possibly contaminated feed solutions. If the TMP increases over time, the resistance increases proportionately, which means the membrane operates above its critical flux.

The concept of critical flux is essential but does not give useful guidance in a practical situation and could not provide a precise suggestion for the operator in the membrane-related industry (Field & Pearce, 2011). By contrast, a more practical concept called a 'threshold flux' is recommended. It was defined as the "flux at or below which a low and near constant rate of fouling occurs but above which the rate of fouling increases significantly (Bacchin et al., 2006)." In other words, threshold flux can be defined as the flux that separates a region of low fouling from a region of high fouling (Bacchin et al., 2006). Thus, the transition between low (negligible) fouling and significant fouling is referred to as the threshold flux. At fluxes below the threshold flux, TMP increases slowly and consistently over time.

Lab-scale fouling experiments are carried out by recording permeate flux loss with time change at a constant TMP (Motsa et al., 2015). When the membrane fouls, the hydrodynamic surroundings and foulant concentration at the membrane surface change, complicating the assessment of fouling behavior. This problem can be solved using constant flux experiments.

2.4.2 Comparison between critical flux and threshold flux

$$\frac{dm}{dt} = 0;\ J_p \leq J_{C,} \quad (2.2)$$

$$\frac{dm}{dt} = B\left(J_p(t) - J_c\right);\ J_p(t) > J_c \quad (2.3)$$

Where m denotes the permeability of the membrane, B denotes a fitting parameter, and $J_p(t)$ denotes the permeate flux at time t.
Equation 2.2 and 2.3 is related to critical flux. Regarding the threshold flux J_{th}, the equations introduced by Field et al. are as follows:

$$\frac{dm}{dt} = a;\ J_p(t) \leq Jth,\ (2.4)$$

$$\frac{dm}{dt} = a + b\left(J_p(t) - J_c\right);\ J_p(t) > Jth,\ (2.5)$$

Where both a and b are both fitting parameters.

By comparing the four formulas, an obvious difference is whether there is an "a" parameter between the threshold flux equation and the critical flux equation. If we assume that a = 0, (2.4) and (2.5) are likely to change to (2.2) and (2.3), respectively. The parameter "a" indicates the constant permeability loss rate of the membrane in the presence of below-threshold flux conditions. If a is equal to zero, there is no loss of permeability over time, meaning no fouling occurs. This is only valid when below critical flux, and (2.4) includes (2.2) if a = [0, ∞).

2.4.3 Factors influencing threshold flux

Numerous factors influence the threshold flux, including the properties of the feed solution and membrane and the hydrodynamics at the membrane surface (Bacchin et al., 2006). The threshold flux increases with larger particles, higher crossflow velocity, and lower feed concentration (Chen, 1998; Metsämuuronen et al., 2002). A decrease in membrane pore size can lower permeate flux and threshold flux (Chen, 1998).

2.5 Membrane and O/W emulsion characterization

2.5.1 Interfacial tension

Interfacial tension is considered one of the key parameters of oil penetration because it affects the deformability of oil droplets and their possibility to pass through the membrane pores. Surfactants such as anionic surfactants can affect surface tension due to hydrophilic head groups and hydrophobic tails. Due to its amphiphilic structure, surfactants tend to accumulate at the interface, which is called adsorption. The surfactant is strongly adsorbed on the interface, thereby reducing the interfacial tension. A contraction force acting on the interface, making the interface as small as possible. Schroder and Schubert also reported that with a high concentration of surfactant, an emulsion is likely to form small droplets and a low concentration leads to larger droplets (Schroder and Schubert, 1998) since with an increase in SDS concentration, it will lead to relatively low interfacial tension by decreasing of interfacial energy due to an increase of interfacial area. Also, a decrease of capillary forces of oil droplets and thus increases the mobility of oil will occur. As a result, the stability of the O/W emulsion will increase. It is also supported by an increase in the absolute value of zeta potential. Moreover, the interfacial tension reduction entirely depends on the amount of surfactant adsorbed at the O/W interface. Surfactant adsorption is a complex phenomenon since

surfactant molecules have to move from the bulk phase to the O/W interface. Many mechanisms may be related to surfactant adsorption, such as electrostatic interaction, van der Waals interaction, and covalent bonding.

2.5.2 Zeta potential

The zeta potential is a physical property that any particle in suspension exhibits and can be used to measure the surface charge and can reflect the stability of O/W emulsion. In other words, it can be used to improve suspension and emulsion formulation. Understanding the zeta potential can help shorten the time required to create trail formulations. It aids in the forecasting of long-term stability. The zeta-potential can be determined based on Laser Doppler Electrophoresis. The zeta-potential is used as a measure for the electrostatic stabilization of particles in a dispersion. Other factors, like, e.g., sedimentation, can also influence the stabilization or de-stabilization of dispersion, and therefore it is possible that the zeta-potential alone does not give enough information whether a dispersion is stable. The value of the zeta-potential depends on the particles, the type of dispersant, and dilution. For example, the zeta potential of SDS-based O/W emulsions is strongly negatively charged, so the zeta potentials range from −70 to −110 mV with increased SDS concentration (Avranas et al., 1988). Similarly, Xin et al. reported that the absolute values of zeta potential of the O/W emulsion increase, and droplet size becomes smaller, and droplet size distribution becomes narrow when SDS concentration increases. O/W emulsions adding SDS are strongly negatively charged, with zeta potentials ranging from −100 to −110 mV (Li et al., 2001; Vácha et al., 2011). O/W emulsions adding CATB are strongly positively charged with zeta potential at +75 mV (Vácha et al., 2011). Besides, according to Tanudjaja et al., with an increase of salts concentration from 50 ppm to 600 ppm, the zeta potential of solution increase from -40 mV to -10 mV (Tanudjaja, H. J. et al., 2017).

Zeta potential is also a significant physical parameter for the membrane. The zeta potential of the membrane is dependent on the pH and ionic strength. Fig.4 illustrates the surface of the SiC membrane is negatively charged when pH larger than isoelectric point, and the membrane had a higher negative zeta potential at higher pH (Nagasawa et al., 2020). Similar findings had been extensively reported. Abro et al. show that the zeta potential of SiC membranes is from -20 to -35 mV with a pH range from 5 to 7 (Abro et al., 2016). Loet al. conducted an experiment to investigate the influence of the pH of O/W emulsion and the crossflow velocity by using a UF membrane. The results show that pH has no effect on the particle size distribution and zeta potential of O/W emulsion, but the zeta potential of membrane changed (Lo et al., 2016). The membrane's zeta potential was also affected by the ionic strength of the solution. The negative zeta potential of the ceramic membrane was greater at 0.1 M ionic strength than it was at 1 M. The smaller absolute zeta potential value is due to compressing the

thickness of the electric double layer (Caltran et al., 2020). For O/W emulsion adding SDS, due to electrostatic repulsion, it is not possible to adsorb surfactant on the surface of the membrane. Moreover, Tanudjaja reported that with an increase of salts concentration from 50 ppm to 600 ppm, the surface potential of membrane increases from -48 mV to -22 mV (Tanudjaja, H. J. et al., 2017).

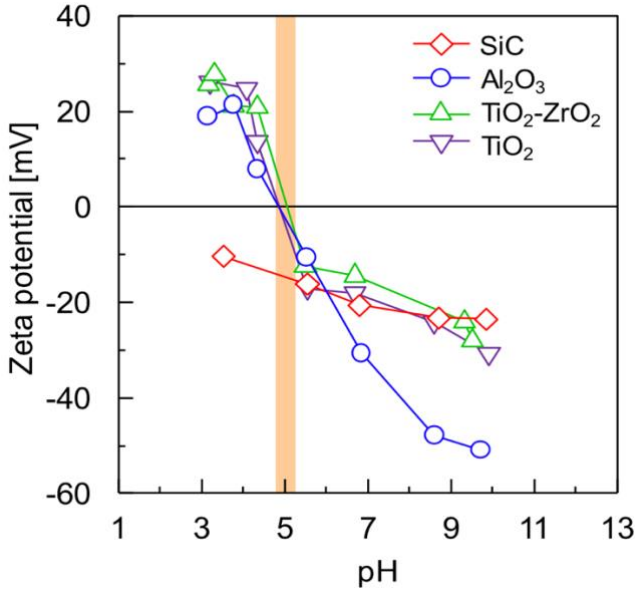

Fig. 4. Zeta potential of the ceramic membrane as a function of the pH (Nagasawa et al., 2020).

2.5.3 Contact angle

The contact angle is determined by the surface of the membrane. The value of the contact angle, which can be regarded as an effective tool to quantify the membrane surface polarity, ranging from 0 to 180. The higher values mean highly hydrophobic surfaces (Hosseinabadi et al., 2014).

2.6 Chemical cleaning

There are two ways to decrease membrane fouling. One is hydraulic cleaning, which includes a forward flush with feed and backwashing with permeate, reducing the reversible fouling. The other is chemical cleaning, which can decrease irreversible fouling.

Before physical cleaning, based on the electrostatic balance model, the reduction of the force to retain foulants on the membrane surface during the cleaning process is the most important step before physical cleaning. Therefore, the choice of cleaning agent should depend on the nature of the foulant (Hakamiet al.,2020). The mechanism of membrane cleaning agents is shown in Table 1.

Table 1. mechanism of membrane cleaning agents.

Cleaning agents	Chemicals	Reactions
Acids	Sulfuric Acid (H_2SO_4)	Solubilization
Base	Caustic soda (NaOH)	Hydrolysis and solubilization
Oxidants	Hypochlorite (HClO)	Oxidation and disinfection
Acid chelate	Citric acid	Chelation
Alkaline chelate	EDTA	Chelation
Surfactants	Proprietary	Surface conditioning

2.7 Chemical Stability

The chemical stability of organic membranes has been well studies. Elshof reported that when membranes are soaking in 1 M HNO_3 and 1 M NaOH for two months, PEM nanofiltration membranes are stable at extreme pH conditions. However, PAH/PAA membranes are not stable at extreme pH conditions (Elshof et al., 2020). Research on the chemical stability of SiC under acid or alkaline solution soaking has attracted widespread attention. The mass loss of the sample gradually increased with the increase of soaking time. However, the rate of SiC falling off becomes slow. The oxidation bonded SiC sample shows good corrosion resistance in long-term experiments. In any case, the loss of quality will not exceed 1% of the total sample mass (Bukhari et al., 2018). Zou et al. reported that α-Al_2O_3 UF membranes are soaking in the H_2SO_4 (pH=1) and NaOH (pH=14) for 24 h, and the weight loss was below 0.1% (Zou et al., 2017). It is reported that SiC is stable at a pH range of 3-10 at 90°C for two weeks. However, it is unstable when soaking in acidic solution (pH=1) due to the formation of surface siloxane groups (Si-O-Si), making SiC dissolve quickly. Na_2 SiO_3 is formed when soaking in NaOH (pH=11) (Das et al., 2018). But Bukhari et al. reported that oxidation bonded SiC MF membrane has good corrosion resistance not only in H_2SO_4 (pH = 2) but also in NaOH (pH=12) for 60 days, which is a suitable technology for harsh wastewater treatment (Bukhari et al., 2018).

2.8 The fouling mechanism of SA

SA is a hydrophilic microbial polysaccharide composed of a linear copolymer, 1,4-linked β-d-mannuronic acid, C-5 epimer, and α-l-guluronic acid in varying proportions (Katsoufidou et al., 2007). The structural formula for SA is shown in Fig. 5.

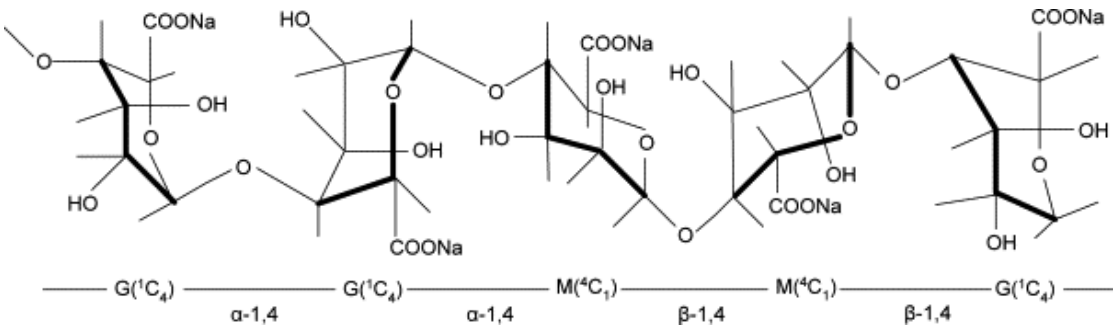

Fig. 5. The structural formula of SA molecule (Katsoufidou et al., 2007)

Physical properties of SA are variable with the characteristics of solution (ionic strength, pH). At a pH of 7, due to deprotonated carboxylic functional groups, the strong negative charge of SA causes repulsive electrostatic interactions between and inside molecules. Besides, in a SA solution, any change in ionic strength significantly impacts polymer chain extension (Ang et al., 2006; Lee et al., 2006). Hering et al. reported that some divalent cations can strongly bind to SA molecules. For instance, Ca^{2+} is highly receptive to carboxylic groups (Hering et al., 1988). As a result, it can complex with the carboxylic groups of SA molecule reduces their negative charges to a certain extent (Tiller et al., 1993). Besides, Ca^{2+} can bind two SA molecules together in an organized manner through the bridging effect, and alginates form complexes with a distinct structure, resulting in a compacted gel network. The gel network is also called "egg-box-shaped gel network" as shown in Fig.6 (Zhang et al., 2016). Therefore, the TMP is affected by the presence of calcium ions and decreases as their concentration increase. This behavior can be explained by the fact that the Ca^{2+} promote the aggregation of the organic macromolecules, resulting in larger effective sizes of the fouling species and thus lower fouling resistances. Other organic foulants have been reported to have similar fouling behavior (Katsoufidou et al., 2005).

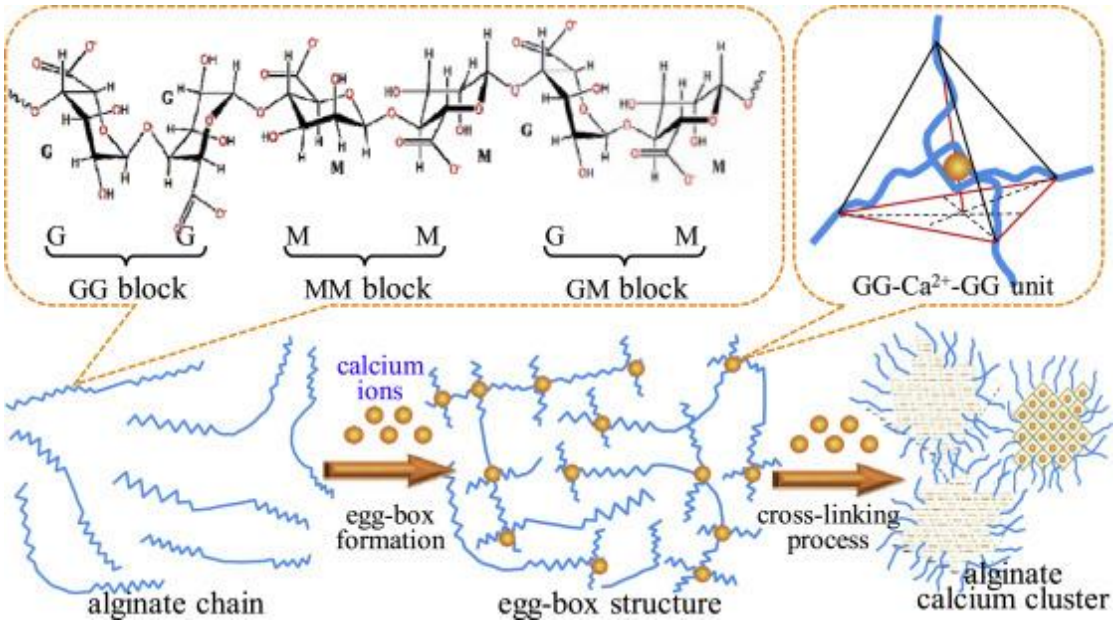

Fig. 6. Sketch map illustrating a cross-linking process of alginate induced by Ca^{2+} (Zhang et al.,2016).

Apart from forming "egg-box-shaped gel network", the change of ionic strength also has a significant effect on the zeta potential of the SA solution. Alresheedi et al. reported that after eight-hour filtration experiments, the SA solution with Ca^{2+} shows a higher increase in TMP compared to the SA solution. Besides, Ca^{2+} reduced the zeta potential of the SA solution. As a result, the fouling rate increases since the electrostatic repulsion forces between alginate and membrane decrease (Alresheedi et al., 2019). This behavior is in line with previous findings on alginate fouling with polymeric membranes (Katsoufidou et al., 2010). This study illustrated that the presence of Ca^{2+} leads to a reduction in the electrostatic repulsion between alginate chains, thereby promoting the formation of coiled alginate macro-molecular structures. Such macromolecules are likely to produce gel layers that are more compact and less permeable (Katsoufidou et al., 2007).

3. Material and methodology

3.1 Materials

As shown in Table 2 and Fig.7a, the SiC UF membrane was used for filtration experiments of SA. This coated membrane produced by LPCVD deposition used commercial tubular ceramic membranes (CoorsTek, the Netherlands) as a support layer at 760 ºC and 860 ºC. The inner diameter and outer diameter were 7 mm and 10 mm, respectively. These membranes were made of α-alumina with a pore size of 100 nm. The pure water permeance at 20ºC (non-fouled) was 382 $Lm^{-2}h^{-1}bar^{-1}$, according to the information provided by the manufacturer. PM, LM, HM are the abbreviation of the pristine membrane, 760 ºC coated membrane, 860 ºC coated membrane, respectively.

Table 2. Characteristics of SiC membrane.

Characteristics of ceramic membrane	LiqTech Ceramics A/S	CoorsTek
Material	SiC	SiC, Al_2O_3
Length, mm	1500, 2500	1500
Outside diameter, mm	8	8
Quantity of channels	1	1
Membrane area, m^2	0.0028	0.003
Pore size, nm	100	40
pH range	0-14	0-14
Operating pressure, bar	1-10	1-10
Maximum temperature, ºC	100	100
Isoelectric point	2.8	-

As shown in Table 2, Fig.7b, and Fig.7c, the membranes used for determining threshold flux were commercial SiC MF membranes (Liqtech Ceramic A/S, Denmark). They were used for the determination of threshold flux. The length of the membranes was 15 cm and 25 cm, and the pore size of the membrane was 100 nm. The inner diameter and outer diameter were 7 mm and 10 mm, respectively. The pure water permeance at 20ºC (non-fouled) was 3000 $Lm^{-2}h^{-1}bar^{-1}$. The membrane surface was negatively charged in the pH range from 3 to 10, which means the isoelectric point of the membrane was lower than 3.

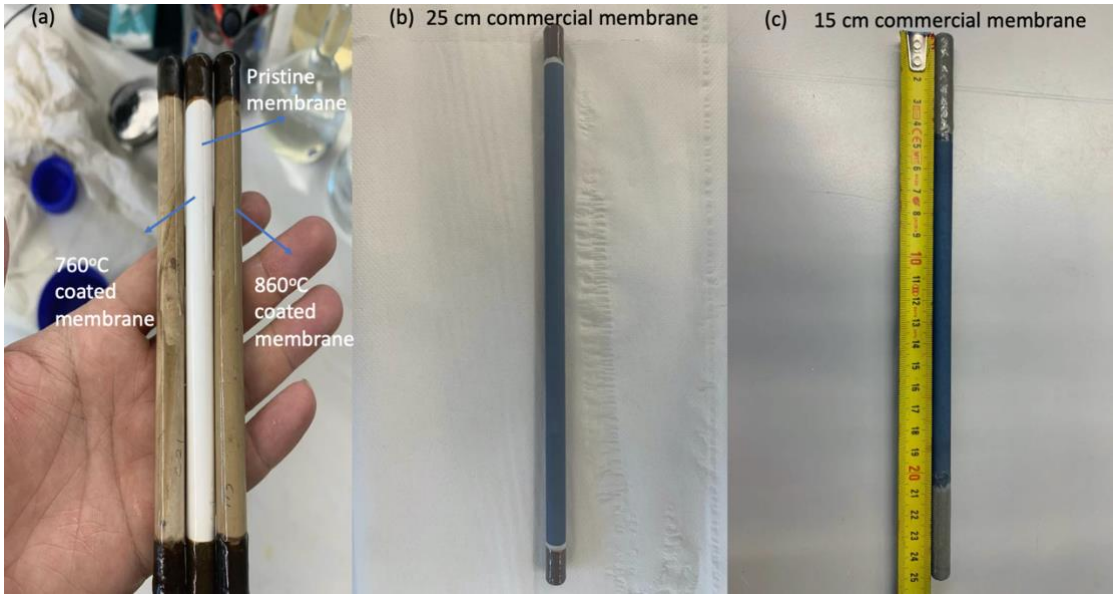

Fig. 7. Photos of the (a) pristine membrane (PM), 760 °C coated membrane (LM), 860 °C coated membrane (HM), (b) 25 cm commercial SiC membrane, (c) 15 cm commercial SiC membrane.

3.2 O/W emulsion formulation

In this study, seven kinds of O/W emulsions were shown in Table 3 were synthesized based on the following procedure. All O/W emulsions were prepared one day before the filtration experiments to ensure emulsions are fresh. The CMC of SDS is 8.2 mM (2364 mg/L). In this research, the concentration of SDS is below the CMC. The pH of demi water was 5.8.

Table 3. Seven kinds of O/W emulsion.

Solution	Oil concentration (mg/L)	SDS (mg/L)	NaCl (mmol/L)	pH
1	400	100	0	5.8
2	400	400	0	5.8
3	400	800	0	5.8
4	400	100	10	5.8
5	400	100	100	5.8
6	400	100	0	3
7	400	100	0	10

3.2.1 O/W emulsion adding SDS

The procedure of preparation of 400 mg/L O/W emulsions with varying SDS concentration (100/400/800 mg/L) is shown as follows: Firstly, the emulsions were made by dissolving 4.5 mL mineral oil (Sigma-Aldrich, Zwijndrecht, Netherlands) and 0.9, 3.6, 7.2 g SDS (Sigma-Aldrich 151213, Zwijndrecht, Netherlands) with 1 L of demineralized water. The O/W emulsions were continuously stirred at 1200 rpm with a magnetic stirrer (L23, LABINCO, the Netherlands) for 48 hours, followed by sonication in a sonifier (Branson Digital) at 40% for 0.5h until it appeared milky white. The emulsion remained stable and homogeneous for three days. Before every experiment, the fresh emulsion was prepared by diluting 1L O/W emulsion to 9L using demineralized water with a constantly desired oil concentration (400 mg/L) since the typical value in produced water is 50 – 500 mg/L (Fakhru'l-Razi et al., 2009).

3.2.2 O/W emulsion adding SDS and NaCl

The procedure of preparation of 400 mg/L O/W emulsions with 100 mg/L SDS and 10 mM/L NaCl is shown as follows: O/W emulsions were made by dissolving 4.5 mL mineral oil, 0.9 g SDS, and 0.59 g NaCl with 1 L of demineralized water. The O/W emulsions were continuously stirred at 1200 rpm with a magnetic stirrer for 24 hours, followed by sonication in Sonifier at 40% for 0.5h until it appeared milky white. Before every experiment, the fresh emulsion was prepared by diluting 1L O/W emulsion to 9L by using 10 mM/L NaCl solution.

3.2.3 O/W emulsion adding SDS and adjusting pH

The procedure of preparation of 400 mg/L O/W emulsion with 100 mg/L SDS and the pH of a solution is 3,10 shown as follows: O/W emulsions were made by dissolving 4.5 mL mineral oil, 0.9 g SDS, and adjusting pH to 10, 3 by adding 1M NaOH and 1M HCl, respectively, with 1 L of demineralized water. The O/W emulsions were continuously stirred at 1200 rpm with a magnetic stirrer for 48 hours, followed by sonication in Sonifier at 40% for 0.5h until it appeared milky white. Before every experiment, the fresh emulsion was prepared by diluting 1L O/W emulsion to 9L by adding 1M NaOH, and eventually, the pH of the emulsion was adjusted to 10. For O/W emulsion adding HCl, the pH eventually reached 3.

3.3 O/W emulsion characterization

As illustrated in Section 2.1, O/W emulsion with adding 100/400/800 mg/L SDS was successfully measured for COD and other chemical and physical parameters. O/W emulsion was characterized by measuring its oil concentration and other physical or chemical parameters.

3.3.1 COD and PSD

Hach-Lange Kits measured COD (mg COD/L). For emulsion, oil concentrations were measured based on the tested COD values. Since O/W emulsion is adding SDS, it is critical to know the relationship between COD values and responding SDS concentrations.

The oil retention for SDS was measured by COD of permeate solution. The oil retention can be defined as:

$$R = \left(1 - \frac{Fp}{Ff}\right) \times 100\% \quad (3.1)$$

Where F_p and F_f are the oil concentration in the permeate and the feed, respectively.
The oil droplet particle size distribution (PSD) was determined with a blue wave Microtrac SDC (Bluewave, Microtrac, USA). The detailed procedure can be seen in Appendix A.

3.3.2 Zeta potential

Zeta potential is a vital physical property that can reflect the stability of colloidal dispersions. The zeta potential of seven samples was measured by a Malvern Zetasizer Nano ZS instrument (Zetasizer lab, Malvern, UK) and determined by equation 3.2.

$$\zeta = \frac{4\pi\eta}{\varepsilon}\frac{\nu}{U/L} \quad (3.2)$$

Where η is the viscosity of water, ε is the dielectric constant of water, ν is the mobile velocity of the oil droplets in the electric field, U is the voltage, and L is the distance between the two electrodes.

A visual inspection of the samples showed that they consist of cloudy dispersions. Under stirring, a sample was taken from the dispersion and injected into the capillary cell. Before the analysis, the capillary cell was rinsed and cleaned with ethanol and subsequently rinsed with the dispersion to be measured. The sample was homogenized, and a sample was taken from the dispersion and injected into the capillary cell (1 mL). The capillary cell was sealed and placed into the Malvern Zeta sizer Nano ZS. The temperature was set at 10°C, the dispersant parameters used are viscosity (0.887 mPa·s),

refractive index (1.33), and dielectric constant (78.5). A dependent triplicate was measured over each sample with a delay between each measurement of 30 seconds to determine the stability of the dispersion, and the samples have been measured as independent duplicates.

3.3.3 Other chemical and physical parameters

The pH of the O/W emulsion was measured by a pH sensor (inoLab™ Multi 3430 - WTW). The TOC (Total organic carbon) concentration of SA was measured by TOC - VCPH analyzer (Shimadzu, JP).

3.4 Preparation of SA solution

In this research, 1.0 g SA power (SA, Sigma-Aldrich 9005383, Zwijndrecht, Nerthrlands) was dissolved in 2L demineralized water and continuously stirred at 1200 rpm with a magnetic stirrer (L23, LABINCO, the Netherlands) for 2 h to dissolve SA totally. After that, to ensure complete mixing, a $CaCl_2$ solution was added to the prepared SA solution and continuously stirred for 22 h. The effect of the presence of sodium ions and calcium ions in SA solution on membrane fouling had been investigated. As shown in Table 4, one concentrations of SA (50 mg/L) and two concentration levels of Ca^{2+} concentration levels (0.1mM, and 1mM) were prepared.

Table 4. SA solution composition and Filtration conditions.

Solution	SA (mg/L)	$CaCl_2 \cdot 2H_2O$ (M)	NaCl (mM)	Flux (LMH)	Filtration type	Time of per cycle	Number of cycles
1	50	-	-	80,90	Dead end	20	4
2	50	1	10	80	Dead end	14	4
3	50	0.1,1	-	90	Dead end	20	4

3.5 Experiment set up

The pressure was measured by two high-precision pressure transducers (GS4200-USB, ESI, UK) during the experiment. The pressure was measured at one location in the system in contrast to three locations for a similar set-up in earlier research. This was done because the pressure difference between both membrane sides can be neglected, and the pressure at the permeate stream is equal to the air pressure.

The feed is pumped through the membrane by a pump (Grundfos, DDA), which was used to set the permeate flux. Besides, the crossflow velocity and forward flush were controlled by a separate pump (Van Wijk & Boersma).

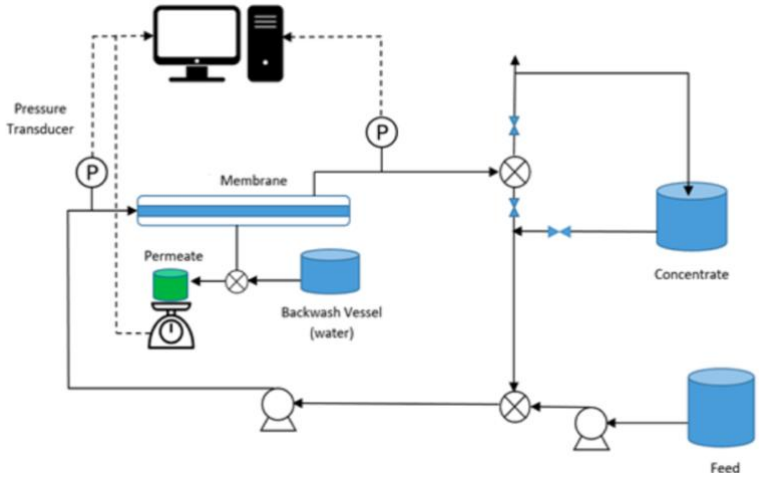

Fig. 8. Experiment set up with constant flow rate

3.6 Filtration test

The fouling resistance of the membrane was conducted by constant flux crossflow experiments. Every filtration experiment started with a pure water permeability test. Pure water fluxes were measured before and after fouling using demineralized water in a crossflow system using a crossflow velocity of 0.44 m/s and TMP is ranging between 0.2 bar and 1 bar due to the different intrinsic membrane resistance. This filtration last for 10 to 15 minutes with constant flux to make sure the membrane was fully cleaned and permeate solution was tested with pH. If the pH value was around 5.8, which was very close to the pH of demineralized water, there was no acid or alkali residue on the membrane. Temperature and pressure will be corrected every day because they will affect permeate flux, and all experiments will be done in duplicate. Each fouling experiment had 3 to 5 cycles with 20 minutes each, and permeability was recorded every 30 seconds. Each cycle included the following stages. The first stage was filtration of foulant at a constant flux of 100 $Lm^{-2}h^{-1}$ for 20 minutes. The second stage was backwashing at 3 bars for 30 seconds for removing reversible fouling. The third stage was forward flush using feed water for 15 s at a crossflow velocity of 1.1 m/s. After every filtration experiment, the experiment set up should be washed for 10 minutes at 8 bars to drain the concentrated water in the pipe. And before the start of the next experiments, air bubbles in the tube were exhausted by washing at 8 bar for 5 minutes.

Between the measurements with foulants, all the fouled membranes were chemically cleaned with a 0.4% NaOH solution, which was filled into the filter and left for 2 hours at 60 ^{o}C. This was followed by filling 3% phosphoric acid and leaving the solution in the filter for a duration of 2 hours at 60 ^{o}C. Besides, thermal cleaning was also a good way to clean the membrane by putting the membranes in the oven under 200 ^{O}C for two hours. After chemical and thermal cleaning, the ceramic membrane was tested the pure

water flux by using demineralized water. And filtration experiments of foulants only started if the flux of the membrane had been recovered. All the filtration experiments of SA were carried out in dead-end filtration mode, and all the filtration experiments of O/W emulsions were carried out in crossflow mode.

3.7 Membrane characterization

The pure water flux of the membrane was determined through filtering demineralized water at a constant TMP of 3 bars before the start of experiments to check whether membranes are fully cleaned. Both permeate fluxes, and the water temperature was recorded every 10 s. The influence of the temperature on the membrane water permeability could be neglected since all membrane permeability was corrected to the equivalent at 20 °C using the equation 3.3 (Song et al., 2016):

$$L_{P,20℃} = \frac{J*e^{-0.0239*(T-20)}}{\Delta P} \quad (3.3)$$

Where $L_{p,20\,°C}$ is the permeability at 20 °C ($Lm^{-2}h^{-1}bar^{-1}$), J is the flux of membrane ($Lm^{-2}h^{-1}$), T is the temperature of water (°C), and ΔP is the measured TMP (bar).

R is the resistance to mass transfer, and μ is the permeate viscosity. The TMP divided by the *R* and μ gave the permeate flux through SiC membranes shown in equation 3.4.

$$J = \frac{TMP}{\mu R} \quad (3.4)$$

3.8 Threshold flux and fouling experiments

In this research, the fouling rate was greater than zero, even at the lowest flux (i.e., 30 MLH), which means critical flux could not be used in realistic operations because industrial operations can rarely achieve zero fouling (Stoller et al., 2013). However, it has been observed that when the permeate flux is lower than a flux, the fouling rate is stable and low instead of zero. Field and Pearce defined this flux as the "threshold flux". In some early studies, it was called "critical flux" (Field & Pearce, 2011; Luo et al., 2014). The threshold flux is also defined as the flux at the linear break point of TMP_{avg} and flux curve (Jiao & Sharma,1994; Choi & Dempsey, 2005). When permeate flux is lower than the threshold flux, the TMP_{avg} increases linearly with permeate flux, and total membrane resistance is constant. When permeate flux is larger than the threshold flux, the TMP_{avg} could not increase linearly with flux, and R_{total} increases as flux increases and becomes flux-dependent (Field & Pearce, 2011; Luo et al., 2014). Industrial membrane filtration usually operates at close to but below the maximum permeate flux, resulting in a low and acceptable fouling rate, and therefore the most economical operation. Therefore, the threshold flux could be a more useful indicator in real membrane operation than the critical flux. A higher threshold flux allows the membrane to operate at a higher permeate flux with a low fouling rate and may extend

the operating time before chemical cleaning or physical cleaning. For membrane-based plant, membranes are usually operated at a constant permeate flux (Miller et al., 2014), so laboratory fouling experiments under constant flux is more practical than testing under constant TMP.

Numerous research has explored methods for determining threshold fluxes (Jiao & Sharma, 1994). Firstly, the threshold flux was commonly and conveniently estimated using the flux stepping method (Cho & Fane, 2002; Choi & Dempsey, 2005; Le et al., 2003; Beier & Jonsson, 2010). In the flux stepping method, the permeate flux is increased stepwise, and simultaneously, the TMP for each flux step is recorded (Choi & Dempsey, 2005; Le et al., 2003; Beier & Jonsson, 2010). There are two ways to calculate and determine the threshold flux. The first way used the average transmembrane pressure (TMP_{avg}). TMPavg was computed as the arithmetic mean of all TMPs measured during the gradual, linear rise in TMP following the first, abrupt surge in flux. However, among the majority of critical flux and threshold flux studies, the criterion for linearity of the TMPavg vs. flux relationship below the threshold flux has not been standardized. Luo et al. reported that the best fit straight line across flux point below the threshold flux was determined by using R^2 coefficients of linear regression greater than 0.99 (Luo et al., 2014). Choi and Dempsey proposed using TMP_{avg} to calculate the practical critical flux when a membrane is filtered with surface waters since fouling rate equals zero could be rarely observed in practice (Choi & Dempsey, 2005). Based on the recent definition of critical and threshold flux, Choi and Dempsey calculated what is currently referred as the threshold flux rather than the critical flux (Choi & Dempsey, 2005). However, normally, the linear break point of TMP_{avg} and flux curve was established by visual observation, which could cause the estimated threshold flux value change.

The second method is calculating the rate of fouling (d(TMP)/dt) at each flux step. The average TMP_{avg} and fouling rate (d(TMP)/dt) at each flux step is then plotted as a function of flux. For 25 cm SiC MF membrane, the threshold fluxes for five conditions were evaluated by flux stepping experiments and calculated by the TMP_{avg} method and fouling rate method. However, the last two conditions had not finished due to the increase of permeability of membrane from 3000 LMH to 4200 LMH. For 15 cm SiC MF membrane, the experiments under different conditions were done only once. The threshold fluxes for seven conditions were successfully evaluated by stepping experiments and were calculated by the TMP_{avg} method. Specifically, for the first 10 minutes, the membrane was operated at a low and steady flux. The flux was raised after 10 minutes and held at a higher level for another 10 minutes. For both 25 cm SiC MF membrane and 15 cm SiC MF membrane, fluxes ranging from 30 LMH to 140 MLH were used in the flux stepping tests, with a step duration of 10 minutes and intervals of 10 LMH. The crossflow velocity is 0.43 m/s, and the Reynolds number is 2530.

Experiments with constant flux and crossflow mode were similar to those with flux stepping, the difference is that for fouling experiments, the permeate flux was fixed at a certain value rather than a changeable value. Constant flux fouling was performed at fluxes above, around, and below the threshold flux, which are 50 LMH, 80 LMH, and 120LMH. Besides, representative results had been presented in Chapter 4.3 and all additional experimental results were provided in Appendix C.1.

3.9 Data analysis

During the constant flux filtration experiments, both pristine Al_2O_3 UF membrane and SiC UF membrane, the TMP increases with an increase of filtration time. In order to better compare the antifouling ability of pristine membrane and SiC UF membrane, the TMP and permeability of the membrane during filtration were normalized to the initial TMP_0 and P_0.

The resistance of the membrane was estimated using the resistance-in-series model (Xing et al., 2019), which is shown in equation 3.5:

$$R_t = \frac{TMP}{\mu J} = R_m + R_r + R_{ir} \tag{3.5}$$

$$R_m = \frac{TMP_0}{\mu J} \tag{3.6}$$

$$R_t = \frac{TMP_1}{\mu J} \tag{3.7}$$

$$R_{ir} = \frac{TMP_2}{\mu J} - \frac{TMP_0}{\mu J} \tag{3.8}$$

$$R_r = R_t - R_m - R_{ir} \tag{3.9}$$

where J is the membrane flux (m/s), TMP is the applied TMP (Pa), and average TMP values collected with stable flux were recorded as TMP_0. TMP_1 is the average TMP at the end of each cycle. TMP_2 is the average TMP after backwash and forward flush. μ is the viscosity of the permeate (Pa·s), R_t (m^{-1}) is the total resistance including intrinsic membrane resistance (R_m), hydraulically reversible resistance (R_r), and irreversible resistance (R_{ir}). R_m was measured by filtering of demineralized water, and R_t was measured based on the final TMP when experiments ended. The fouled membrane was backwashed with demineralized water under a pressure of 3 bar for 30 seconds, and then R_{ir} was calculated. Finally, the R_r was calculated from $R_t - R_{ir} - R_m$. R_{ir} is important since the irreversible fouling is hard to be fully cleaned by backwash. The reversible fouling will increase energy consumption since higher pressure is required during backwash with higher R_r.

4. Results and discussion

4.1 O/W emulsion as foulant

4.1.1 O/W emulsion characterization

4.1.1.1 COD and PSD

COD and PSD are two essential parameters for O/W emulsion characterization. The COD and PSD of feed solutions are shown in table 5. The PSD of oil droplets had been well controlled in the range of 1-10 μm in all conditions. It was reported that when the SDS concentration increased, the PSD became narrow, which would lead to relatively low interfacial tension by decreasing interfacial energy due to an increase of interfacial area (Schroder and Schubert, 1998). But in this study, the conclusion contradicted it since high surfactant concentration led to larger droplets. Besides, the PSD of O/W emulsion droplets showed no obvious variation under pH = 3, 5.8,10. The average size of droplets under different pH values shown in Table 5 was consistent with the finding of Lobo et al. (Lobo et al., 2006). With the increase of salinity, the PSD was also in the range of 1-10 μm, which showed that ionic strength had no influence on the PSD of O/W emulsion.

Table 5. COD and PSD of seven samples.

Sample	COD (mg COD/L)	PSD (μm)
400 mg/L oil+100 mg/L SDS	1400	1-10
400 mg/L oil +400 mg/L SDS	2000	1-10; 100
400 mg/L oil +800 mg/L SDS	2800	1-10; 100
400 mg/L oil+100 mg/L SDS (pH=3)	1400	1-10
400 mg/L oil + 400 mg/L SDS (pH=10)	1400	1-10
400 mg/L oil + 100 mg/L SDS +10 mM NaCl	1400	1-10
400 mg/L oil + 100 mg/L SDS + 100 mM NaCl	1400	1-10

Based on the prepared SDS solutions with four different concentrations and the corresponding COD values measured by Hach kits, the relation was plotted in Fig. 9 below. The two parameters show liner relation, which can be explained by equation 4.1 below, with an R^2 value of 1. By using this line, the amount of residue SDS in permeate solution under different fluxes can be calculated as shown in Appendix B.5.

$$SDS = 2.0024 \times Conc._{SDS} + 4.078 \quad (4.1)$$

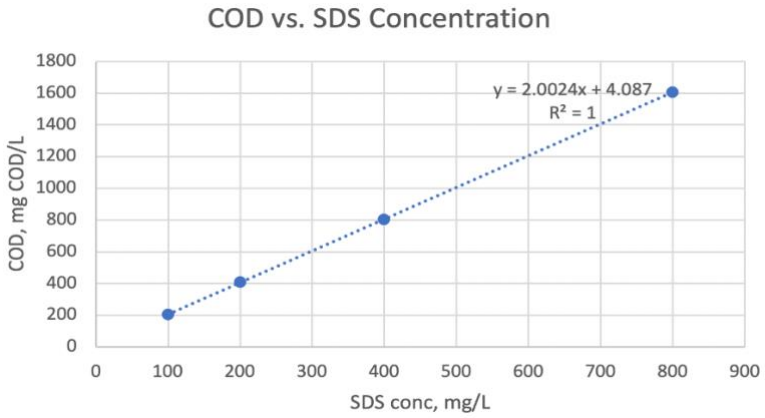

Fig. 9.The relation between COD and SDS concentration

4.1.1.2 Factors influencing particle size distribution

Table 6 showed that with increased mixing time from 24 h to 48h, the COD of O/W emulsion increased from 1254 mg COD/L to 1456 mg COD/L. With increased sonication strength, the range of particle size distribution (PSD) decreased, and COD kept constant, whereas with the increase of sonication time, both PSD and COD kept constant. When O/W emulsion stood for 12 hours or 24 hours, COD and PSD of emulsions remained unchanged compared with the original emulsions, which showed that emulsions were stable.

Table 6. Particle size distribution of seven samples.

Sample	COD (mg COD/L)	PSD (μm)
Mixing (24h) +Sonication (40%/30min)	1254	1-10
Mixing (48h) +Sonication (40%/30min)	1456	1-10
Mixing(24h) + Sonication (40%/30min) + standing time (12h)	1230	1-10
Mixing(24h) + Sonication (40%/30min) + standing time (24h)	1223	1-10
Mixing (24h) + Sonication (40%/30min + standing time (24h) + Dilution(9x)	1352	1-10
Mixing (24h) +Sonication (40%/30min) + standing time (24h) + Dilution(9x) + standing time (6h)	1320	1-10

4.1.1.3 Zeta potential of O/W emulsion

As shown in Table 7, an increase in SDS concentration would lead to relatively low interfacial tension by decreasing interfacial energy due to the increased interfacial area. Also, a decrease of capillary forces of oil droplets and thus increased the mobility of oil will occur. As a consequence, the stability of the O/W emulsion would increase. It was also supported by an increase in the absolute value of zeta potential. With further

increase of SDS concentration from 400 mg/L to 800 mg/L, the absolute value of zeta potential increased until to a constant value since interfacial tension was not changing anymore. Different salt concentrations were used to simulate the zeta potential of different salinity conditions since salts have commonly existed in oily wastewater. It was impossible to measure the zeta potential of the solution with 1M NaCl since it was beyond the instrument's measurement range. With an increase of salt concentration, both the mobility of particles and the absolute value of zeta potential decreased due to the compression of the electrical double layer. The low absolute value of zeta potential led to low droplet-droplet electrostatic repulsion and increased flocculation/coalescence and creaming (the rise of oil flocs or coalesced oil in a gravitational field, suggesting that the high salinity was not conductive to O/W stability. And also, there was considerably less change in zeta potential when the pH of the O/W emulsions was adjusted to 3 or 10, and Prathapan et al. reported a similar finding showed that when O/W emulsion was acidic or basic, the absolute value of zeta potential kept stable (Prathapan et al., 2016).

Table 7. Zeta potential of O/W emulsion.

Sample name	Average Zeta Potential (mV)	Standard Deviation (mV)	Conductivity (mS/cm)
1: 400mg/L oil + 100 mg/l SDS	-91.3	6.7	0.25
2: 400mg/L oil + 400 mg/l SDS	-106.5	2.4	0.43
3: 400mg/L oil + 800 mg/l SDS	-107	3.1	1.26
4: 400mg/L oil + 100 mg/l SDS + 10 mmol/L NaCl	-90.8	4.3	1.62
5: 400mg/L oil + 100 mg/l SDS + 100 mmol/L NaCl	-68.0	2.5	12.15
6: 400mg/L oil + 100 mg/l SDS (pH = 3)	-86.2	3.3	0.31
7: 400mg/L oil + 100 mg/l SDS (pH = 10)	-85.9	2.3	0.26

4.1.2 Threshold flux

4.1.2.1 The effect of SDS concentration and salinity on threshold flux

In this study, as described in Section 3.1, the 25 cm SiC MF membrane was used to investigate the effect of SDS concentration and salinity on threshold flux. Besides, the initial flux was 30 LMH with an increase of constant step length (10 LMH) until a final flux of 140 LMH. During each flux step, the change of TMP was recorded. At the initial stages of flux, no fouling occurred so that the TMP_{avg} of filtering O/W emulsions was close to that of pure water. The reversible fouling could be backwash, and irreversible

fouling was negligible. Thus, there was no accumulative fouling during these fluxes. When flux increased beyond the threshold flux, the accumulation of oil droplets led to a nonlinear relationship between the flux and TMP. Similar observations had been reported elsewhere (Stoller et al., 2013).

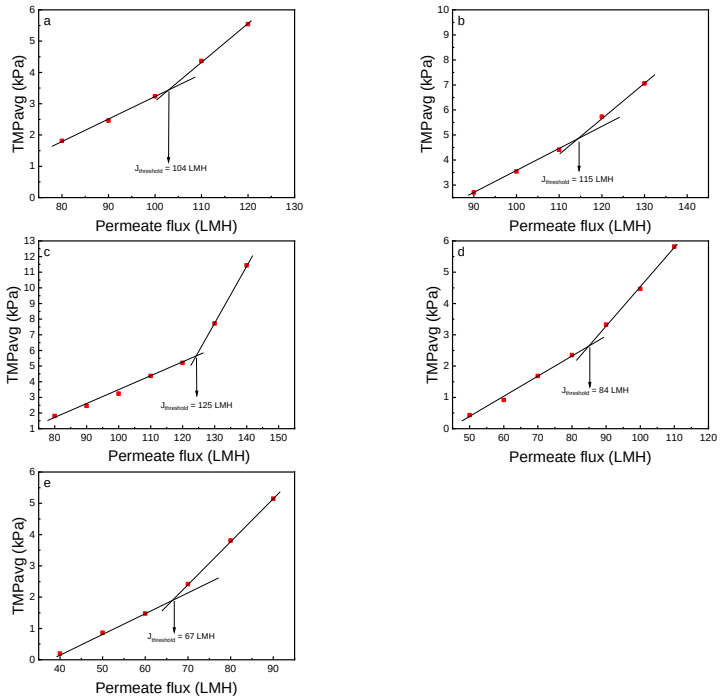

Fig. 10. The TMP_{avg} vs permeate flux for 25 cm SiC MF membrane filtering 400 mg/L O/W emulsion and (a) 100 mg/L SDS; (b) 400 mg/L SDS; (c) 800 mg/L SDS; (d) 100 mg/L SDS, 10 mM NaCl; (e) 100 mg/L SDS, 100 mM NaCl.

TMP_{avg} values at each flux for filtering 400 mg/L O/W emulsions with 100 mg/L SDS had been shown in Fig. 10a. With fitting more TMP data, the R^2 coefficient would decrease. Therefore, the data points were connected by line until the R^2 value began to fall. For fluxes less than 100 LMH, all TMP_{avg} values are contained within a single linear regression with an R^2 coefficient of 0.99 or greater, showing that at these fluxes, the resistance remained constant. When the flux was above 100 LMH, the slope of the TMP_{avg} vs. flux relationship increased since the resistance was increasing. The flux at which the slope changed, 104 LMH, was identified as the threshold flux based on the TMP_{avg} method. As illustrated in Fig.10a and Fig.10b, when the SDS concentration increased from 100 mg/L to 400 mg/L, the electrostatic repulsion between the negatively charged oil droplet and the negatively charged membrane surface increased due to an increase of the absolute value of zeta potential, causing the threshold flux to rise to 115±1 LMH. As shown in Fig.10b and Fig.10c, when SDS concentration was further increased to 800 mg/L, although the zeta potential of O/W emulsion remained constant compared with 400 mg/L SDS, threshold flux still increased to 129±5 LMH due to an increase of particle size distribution of oil droplet. As a result, the antifouling

ability of the membrane enhanced, and threshold flux increased (de Vos and Lindhoud, 2019). As shown in Fig.10d and Fig.10e, with the increase of salinity, threshold flux decreased from 84 LMH to 67 LMH mainly because the mobility of particles decreased, and positively charged ions (Na^+) could screen the negatively charged SDS head groups, reducing the electrostatic repulsion and compressing the electrical double layer. The TMP increased with increasing salt concentration from 10 mM to 100 mM, implying more extensive fouling (Li et al., 2010; Vigneswaran and Kwon, 2015).

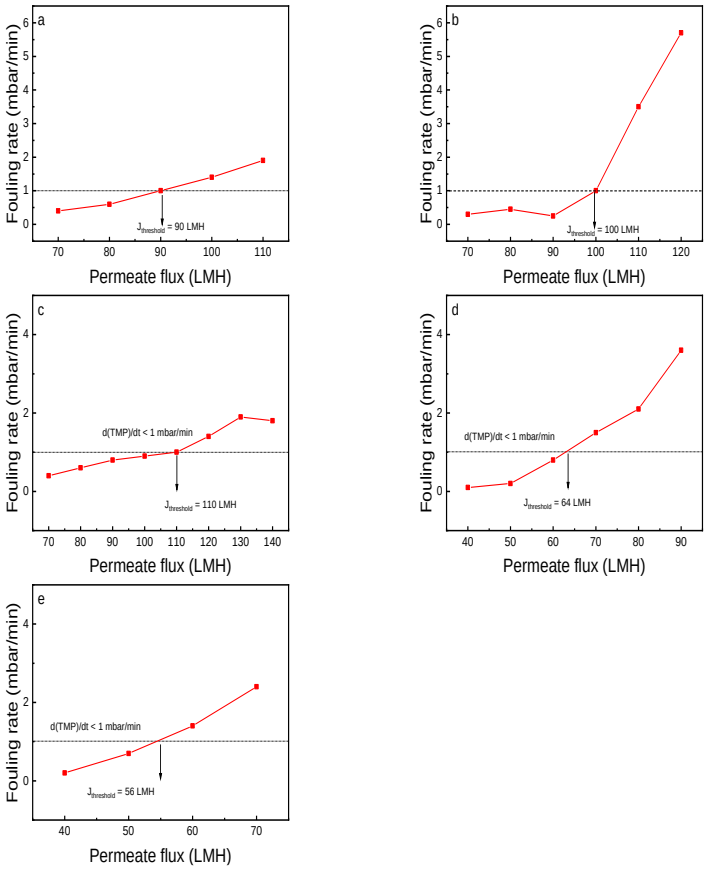

Fig. 11. The fouling rate vs permeate flux for 25cm SiC MF membrane filtering 400 mg/L O/W emulsion and (a) 100 mg/L SDS; (b) 400 mg/L SDS; (c) 800 mg/L SDS; (d) 100 mg/L SDS, 10 mM NaCl; (e) 100 mg/L SDS, 100 mM NaCl.

When filtering 400 mg/L O/W emulsions with 100 mg/L SDS, Fig.11 showed the rate of fouling (d(TMP)/dt) as a function of flux. When the flux was lower than the threshold flux, the fouling rate, defined as 1mbar/min in this case, was low and constant (Torre et al., 2009; Dereli et al., 2014). As shown in Fig.11a, the fouling rate was below 1mbar/min until flux reaches 90 LMH. A dramatic increase in fouling rate could be seen from 80 LMH to 90 LMH and then further increased in fouling rate beyond 1 mbar/min from 90 LMH, suggesting that the flux had exceeded the threshold flux (Dereli et al., 2014). As a result, the threshold flux (denoted by a vertical arrow) was determined to be 90 LMH using this method. As shown in Fig.11a and Fig.11b, when increasing the SDS concentration from 100 mg/L to 400 mg/L, the electrostatic

repulsion between oil droplet and membrane surface increased so that threshold flux further increased to 110±14 LMH. As shown in Fig.11c and Fig.11d, when SDS concentration further increased to 800 mg/L, although the zeta potential of O/W emulsion remained constant compared with 400 mg/L SDS, threshold flux still increased to 117±9 LMH due to an increase of particle size distribution of oil droplet. As a result, the membrane fouling had been alleviated. As shown in Fig.11d and Fig.11e, threshold flux decreased from 64 LMH to 56 LMH since the mobility of particles decreased with increasing salinity, and positively charged ions (Na^+) could screen the negatively charged SDS head groups, reducing electrostatic repulsion and compressing the electrical double layer. The TMP increased as the salt concentration increased from 10 to 100 mM, implying increased fouling (Li et al., 2010; Vigneswaran and Kwon, 2015).

4.1.2.2 The effect of pH on threshold flux

The 15 cm SiC MF membrane was used to investigate the effect of pH on threshold flux. As shown in Fig.12a and Fig.12b, when the pH of the emulsion was adjusted from 5.8 to 10, the negative surface charge of the membrane increased, and stronger electrostatic repulsion happened. At the same time, the inter-droplet repulsion prevented the deposition of particles, thus resulting in the reduction of the thickness of the cake layer. As a result, the cake layer became more “open” and TMP increased slowly. The threshold flux increased from 95 LMH to 113 LMH. As shown in Fig.12c, with higher pH, the threshold flux decreased from 95 LMH to 84 LMH since the negative surface charge of the membrane increased, lowering electrostatic repulsion. It could be concluded that higher pH values led to higher threshold fluxes.

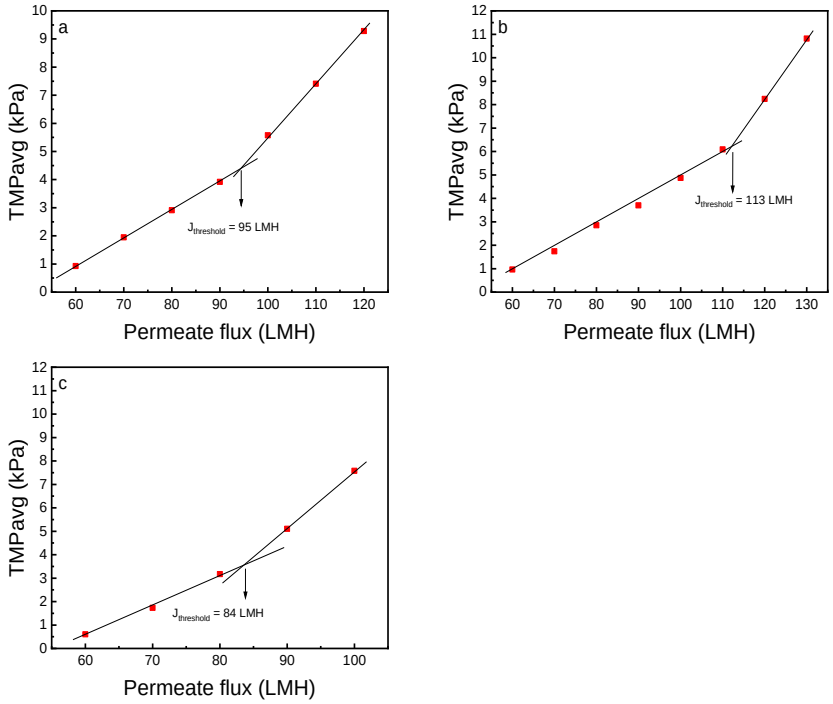

Fig. 12. The TMP_{avg} vs permeate flux for 15 cm SiC MF filtering 400 mg/L oil and (a) 100 mg/L SDS; (b) 100 mg/L SDS, pH = 10; (c) 100 mg/L SDS, pH = 3.

The overview of threshold flux for 15 cm and 25 cm SiC MF membrane under different conditions had been shown in Appendix C.4. Compared with 25 cm SiC MF membrane, 15 cm SiC MF membrane had a lower threshold flux in each condition since the length of 15 cm SiC MF membrane was much shorter, affecting TMP and mass transfer coefficient (Taha & Cui, 2002). Besides, the threshold fluxes measured by the TMP_{avg} method were larger than the fouling rate method for 25 cm SiC MF membrane. One possible explanation is that the fouling rate, defined as 1 mbar/min, was a little bit lower in this study, leading to a lower threshold flux compared with the TMP_{avg} method.

4.1.3 Verification of threshold flux

As mentioned by Beier and Jonsson, the validation of threshold flux could be achieved with constant flux fouling experiments (Beier and Jonsson, 2010). Constant flux fouling experiments were performed at three fluxes: 50, 80, and 120 LMH, representing one flux above and two fluxes below the calculated threshold flux (95 LMH) to compare the fouling behavior of the O/W emulsions. As shown in Fig.13, when flux increases, the initial TMP (The TMP obtained at required flux) increased in proportion to the flux. Below the threshold flux, TMP increased slightly, and above the threshold flux, fouling was severe, and the TMP increased rapidly. Since the permeate flux was constant, the TMP increased since fouling increased the mass transfer resistance.

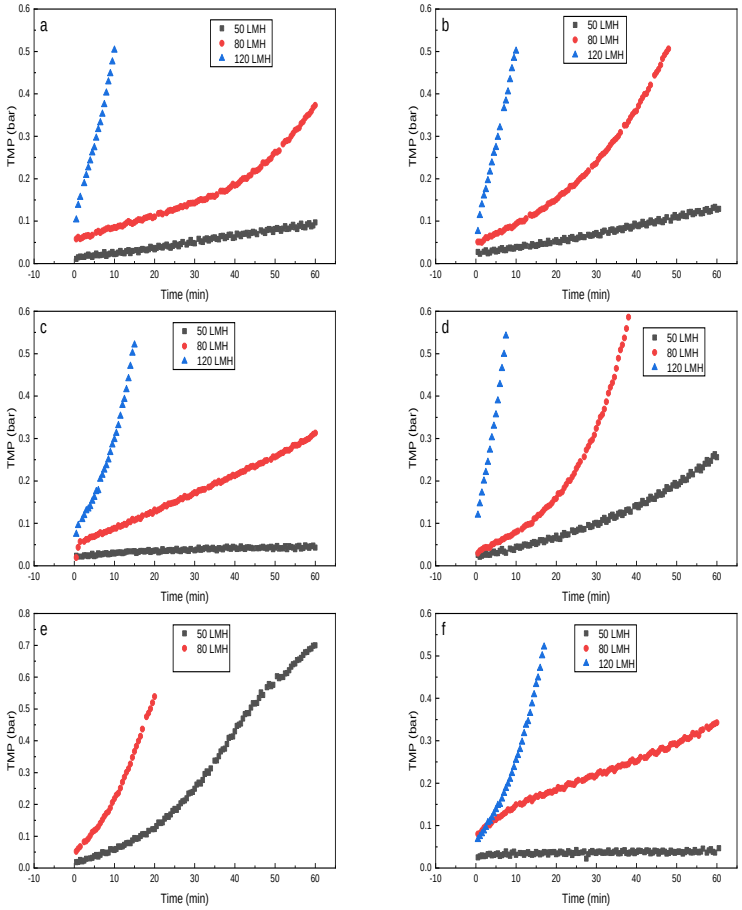

Fig. 13. TMP as a function of time at fixed flux for 15 cm SiC MF membrane filtering 400 mg/L Oil and (a) 100 mg/L SDS; (b) 100 mg/L SDS, pH = 3; (c) 100 mg/L SDS, pH = 10; (d) 100 mg/L SDS, 10 mM NaCl; (e) 100 mg/L SDS, 100 mM NaCl; (f) 400 mg/L SDS.

As shown in Fig.13a, Fig 13b, Fig 13c, Fig 13f, membranes operated at 50 LMH showed the slow, linear TMP rise, indicating that minor fouling happened in membranes (Ho & Zydney, 2002). Marshall et al. reported that, even at extremely low fluxes, some fouling of UF and MF membranes could not be avoided during start-up (Marshall et al., 1996). Membranes operated at 80 LMH, which was slightly less than or more than the threshold flux, demonstrated an intermediate linear increase in TMP during the first few minutes, followed by a rapid increase, which could be explained by the accumulation of oil droplets on the membrane surface and formation of the cake layer, followed by droplet condensation due to the increase of pressure drop across the cake layer. When the membrane operated at a flux of 120 LMH, which was above the threshold flux, the exponential TMP curve showed that foulants were transported to the membrane surface at a rate faster than crossflow shear forces could remove them, possibly leading to oil droplets spreading along the membrane surface, which was also called membrane wetting and this could be distinguished by irreversible fouling (Ye et al., 2005). Kovalsky & Waite reported a similar exponential TMP shape (Kovalsky & Waite, 2009). The increase in the TMP profile was most likely caused by the onset of

cake formation, which increased the resistance to water transport through the membrane (Ho & Zydney, 2002). To keep a constant permeate flux, the TMP increased in lockstep with the resistance increase. The resistance continued to rise as foulants accumulated on the cake layer, and the experiment stopped when the TMP reached its maximum value.

Fig.13c showed that when pH increased to 10, although the zeta potential of O/W emulsion was kept constant, the zeta potentials of membrane decreased with increased pH so that membranes were highly negatively charged, and the electrostatic repulsion became stronger. As a result, TMP increased slowly. However, if pH decreased to 3, the acidification of the O/W emulsion led to weak electrostatic repulsion, thus higher fouling was observed. An increase of salinity of O/W emulsion, as shown in Fig. 13d and Fig. 13e, could have a significant influence on membrane fouling even at a low flux (50 LMH), which could be explained by a reduction of electrostatic repulsion between the oil droplets in the cake layer and were situated closer since the stronger drag forces were generated at a high flux (80LMH), leading to severe fouling (Nabi et al., 2000).

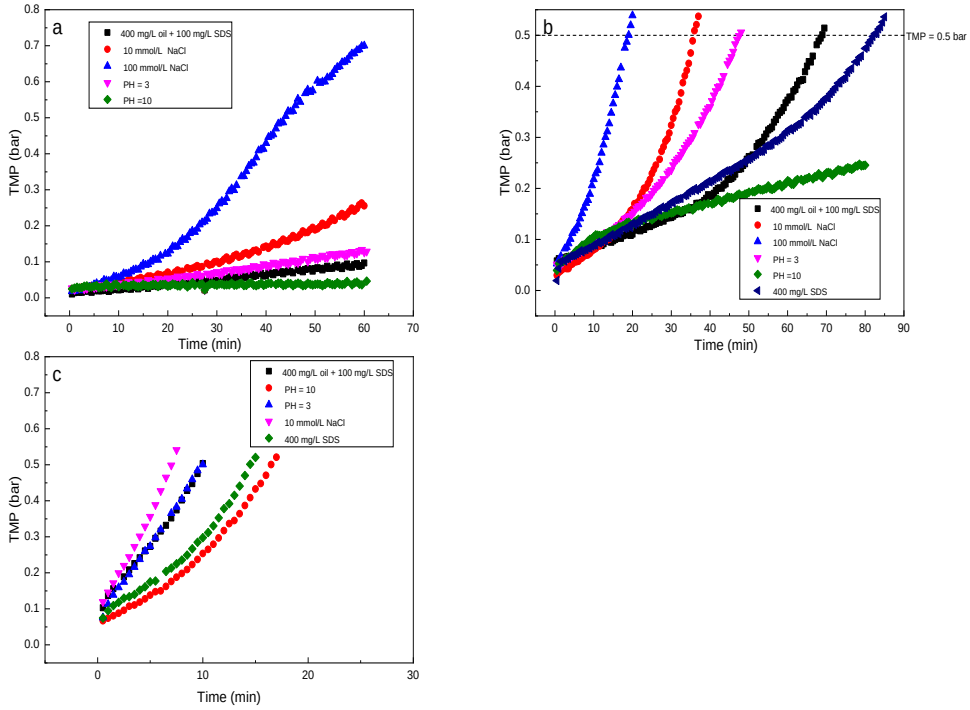

Fig. 14. TMP as a function of time at a permeate flux of (a) 50 LMH, (b) 80 LMH, (c) 120 LMH.

All conditions showed a low and constant fouling behavior during constant flux fouling at 50 LMH except for O/W emulsion adding 100 mmol/L NaCl, as shown in Fig.14a. However, when flux reached 80 LMH, as shown in Fig.14b, all conditions showed a more dramatic increase in TMP than at 50 LMH. At higher fluxes, this change in fouling behavior resulted in a rapid increase in fouling rate. And this result was consistent with

Field's theory (Field & Pearce, 2011), which showed that below the threshold flux, a low and constant fouling rate occurred, and above the threshold flux, the rate of fouling substantially increased.

With an increase of salt concentration, the mobility of particles decreased, and positively charged ions (Na^+) could screen the negatively charged SDS head groups, reducing the electrostatic repulsion and compress the electrical double layer. The TMP increased with increasing salt concentration, implying more extensive fouling, which was consistent with the findings of other similar studies (Li et al., 2010; Vigneswaran and Kwon, 2015).

4.1.4 Relationship between threshold flux and Zeta potential

Fig.15a showed that the change of absolute value zeta potential was consistent with the change of threshold flux, which meant that an increase of the absolute value of zeta potential led to an increase of threshold flux. Fig.15b, two data (pH = 3 and pH = 10) were added, and the threshold flux increased from 80 LMH to 100 LMH when pH increased from 3 to 10. Although the zeta potential of oil emulsion could not change, the surface charge of the membrane was improved at higher pH. Thus higher threshold flux was observed due to stronger electrical repulsion (Lo et al., 2016).

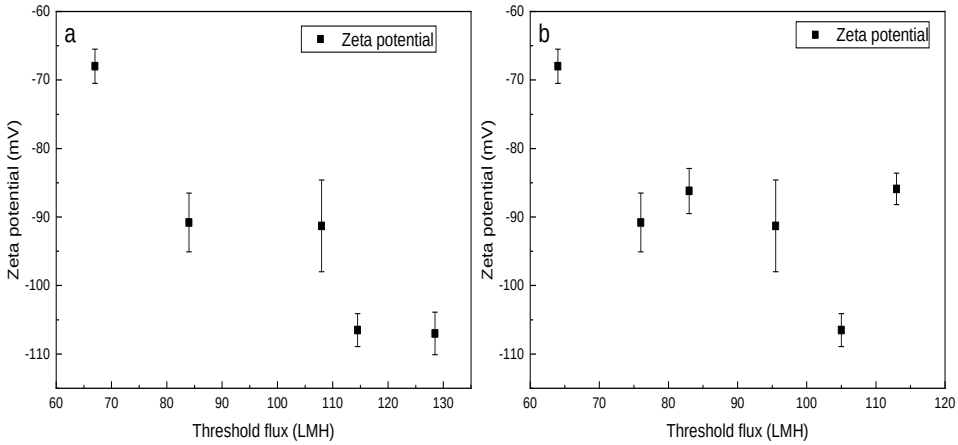

Fig. 15. Relationship between threshold flux and zeta potential for (a) 25 cm SiC MF membrane and (b) 15 cm SiC MF membrane.

4.1.5 COD Retention

As shown in Fig.16, the COD concentration increased as flux increased in the SDS-containing system so that COD retentions decreased with an increase of flux. Under higher filtration flux, greater dilution of surfactant in the permeate could happen. At the same time, filtration at a greater flux level resulted in increased fouling on the membrane surface (Shang et al., 2014). However, the later effect appeared dominant in this case.

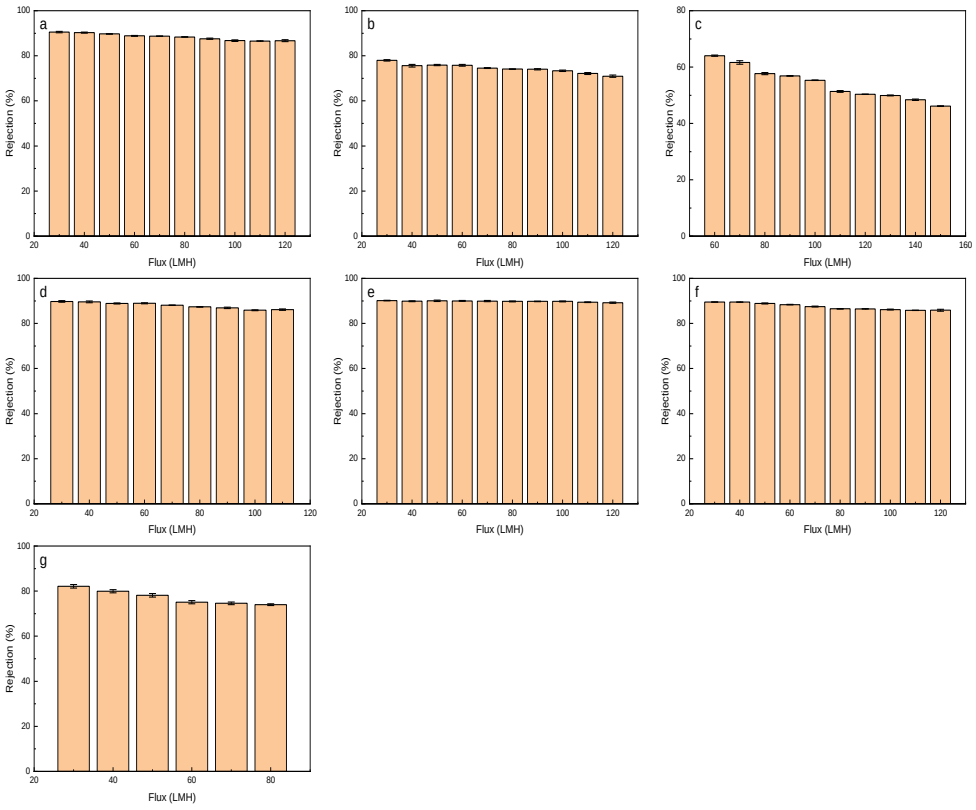

Fig. 16. Oil retention for 15 cm SiC MF membrane filtering 400 mg/L oil and (a) 100 mg/L SDS, pH=5.8; (b) 400 mg/L SDS; (c) 800 mg/L SDS; (d) 100 mg/L SDS, pH = 3; (e) 100 mg/L SDS, pH = 10; (f) 100 mg/L SDS, 10 mM NaCl; (g) 100 mg/L SDS, 100 mM NaCl.

As shown in Fig.16a, Fig.16d, and Fig.16e, the COD retentions were not affected by pH mainly because although a decrease of pH reduced the electrostatic repulsion between the negatively charged oil droplet and negatively charged membrane, oil droplet deformation occurred. However, it was hard to penetrate the pore of the membrane since TMP was still lower than the critical pressure. As shown in Fig.16a, Fig.16b, and Fig.16c, when surfactant concentration increased from 100 mg/L to 800 mg/L, COD retentions decreased from 88.8% to 64.0% at 30 LMH as more SDS molecules in the 800 mg/L feed solution, which could pass through the membrane easily. This was to be expected when the surfactant concentrations employed were lower than the CMC and O/W interface was not saturated. As shown in Fig.16g, the oil retentions were poor at high salinity (100 mM). The reason was that adding salts led to

reduction of interfacial tension and the repulsion between the head group, screening the electrostatic interaction and allowing SDS molecules to be absorbed, and making oil droplet deformation much easier (Zhu et al., 2017). As a result, the membrane surface was more likely to be wetted. The COD concentration of 100 mg/L SDS was 204 mg/L, and in permeate, the COD concentration exceeded 300 mg/L, which also suggested that the oil droplet penetrated the membrane and eventually permeated the solution. Virga et al. reported that an increase of interfacial tension force increases oil retention (Virga et al., 2020). With increased salt concentration from 10 mM to 100 mM, the oil retention reduced from 86.5% to 73.9% at 80 LMH. Besides, at high salinity (100 mM), there was a dramatic decrease of oil retention from 78.5% to 75.1% if the flux was higher than the threshold flux.

4.2 SA as foulant

4.2.1 TMP and fouling resistance

All experiments are shown in Fig.17 – Fig.22 were conducted in dead end mode. PM, LM, HM are the abbreviation of the pristine membrane, 760 ^{o}C coated membrane, 860 ^{o}C coated membrane, respectively. As shown in Fig.17, compared with HM, the TMP of PM increased more rapidly, and fouling resistance was larger. As mentioned in chapter 3.1, the isoelectric point of the SiC membrane is 2.8, whereas the alumina membrane has a higher isoelectric point which is 9. The pH of the SA solution is 5.8, which means that PM was positively charged, and HM was negatively charged during the filtration process. Therefore, the electrostatic repulsion will slow the increase of TMP for HM and decrease the fouling resistance.

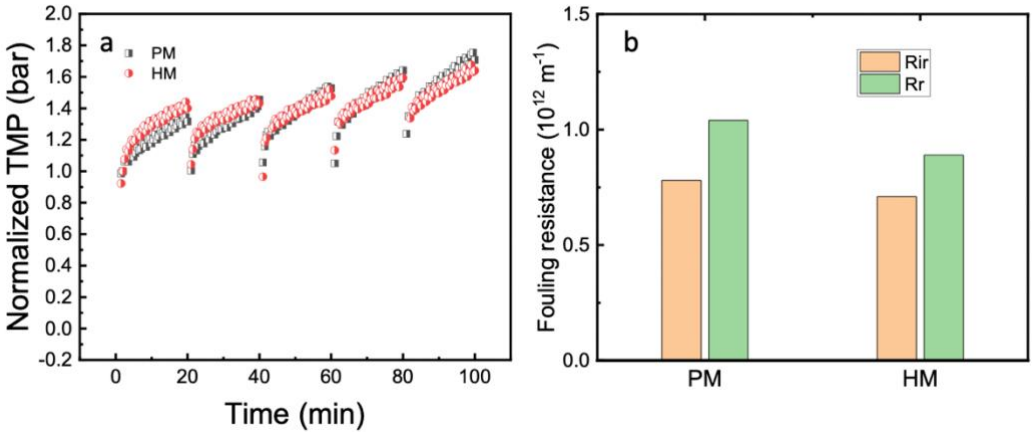

Fig. 17. (a) The TMP_{avg} vs. permeate flux and (b) the fouling resistance for pristine membrane (PM), 860 ^{o}C coated membrane (HM) filtering 50 mg/L SA at 80 LMH.

As shown in Fig.17 and Fig.18, with an increase of permeate flux, compared with HM, the TMP of both PM and HM increased more rapidly, and fouling resistance also increased. This result could be explained by increased fluxes brought more foulant to

the membrane surface, resulting in increased foulant accumulation on the membrane (Miller et al., 2014).

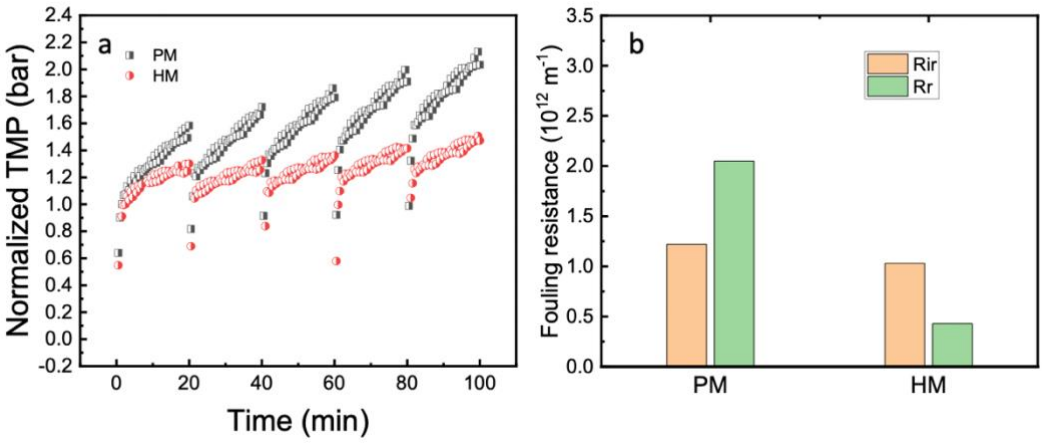

Fig. 18. (a) The TMP_{avg} vs. permeate flux and (b) the fouling resistance for pristine membrane (PM), 860 °C coated membrane (HM) filtering 50 mg/L SA with at 90 LMH.

As shown in Fig.19 and Fig.20, the presence of Ca^{2+} in low ionic strength (0.1 mM and 1mM) could decrease irreversible fouling and increase reversible fouling. This behavior could be explained by the effect of Ca^{2+} on the aggregation of the SA, resulting in larger effect sizes of the fouling species deposited on the membrane surface and forming a loose deposit which could explain irreversible fouling decrease (Lee et al., 2006).

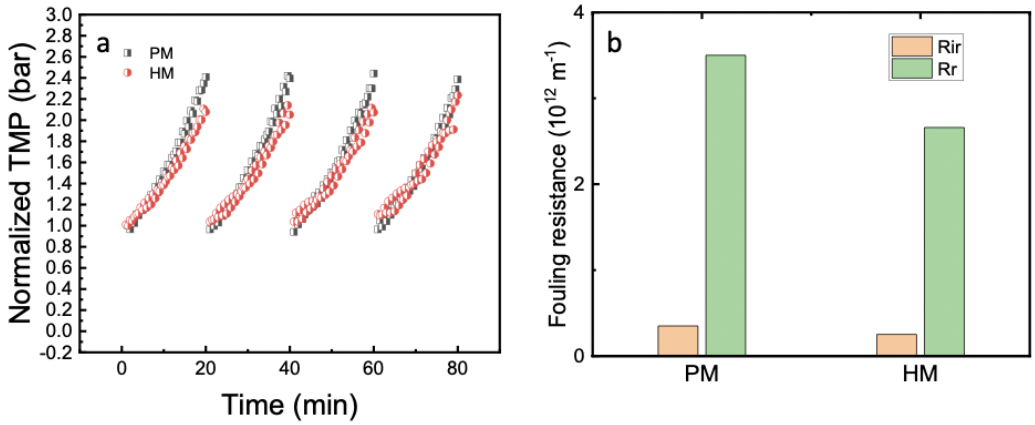

Fig. 19. (a) The TMP_{avg} vs. permeate flux and (b) the fouling resistance for pristine membrane (PM), 860 °C coated membrane (HM) filtering 50 mg/L SA and 0.1 mM $CaCl_2$ at 90 LMH.

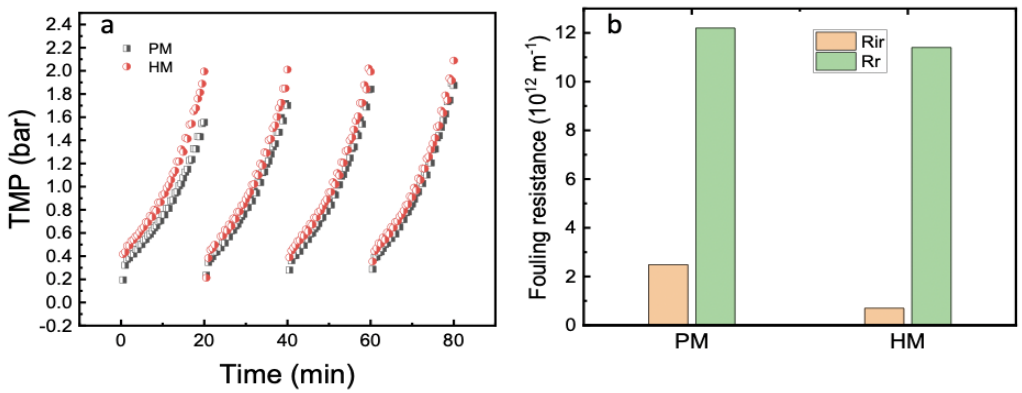

Fig. 20. (a) The TMP_{avg} vs. permeate flux and (b) the fouling resistance for pristine membrane (PM), 860 °C coated membrane (HM) filtering 50 mg/L SA and 1 mM $CaCl_2$ at 90 LMH.

Fig.21 illustrated that when pH equaled to 3.6, the irreversible fouling was dominant at the lower pH, showing that the protonated alginate was more attracted to the membrane surface than the deprotonated alginate.

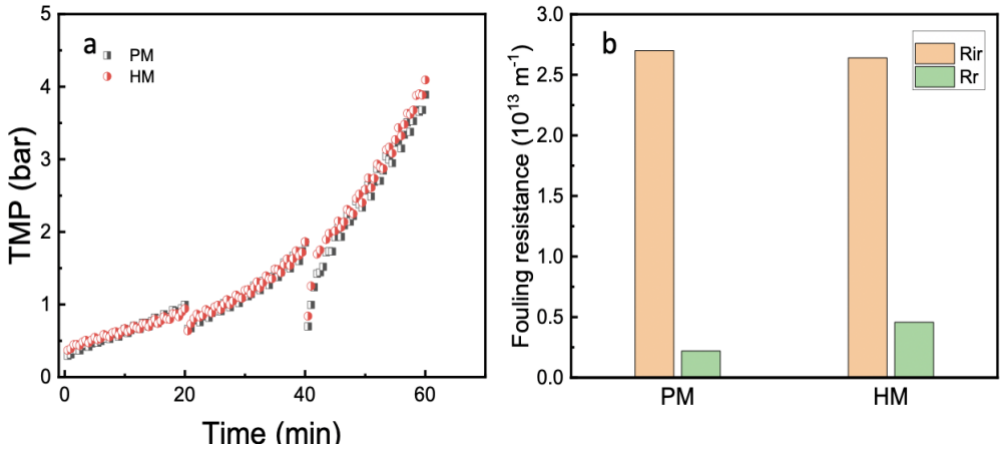

Fig. 21. (a) The TMP_{avg} vs. permeate flux and (b) the fouling resistance for pristine membrane (PM), 860 °C coated membrane (HM) filtering 50 mg/L SA at 80 LMH, pH = 3.6.

Fig.22 showed that with increased ionic strength by adding 10 mM NaCl and 1 mM $CaCl_2$, TMP increased rapidly compared with pure SA solution or SA solution adding calcium ions since charges on both alginate and membrane were reduced through double layer compression and charge screening, resulting in decreased electrostatic repulsion between alginate molecules and the membrane surface.

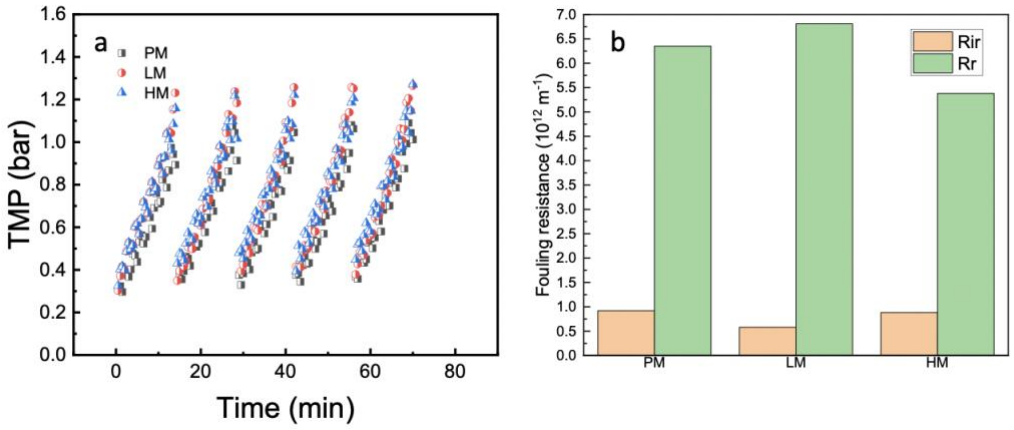

Fig. 22. (a) The TMP_{avg} vs permeate flux and (b) the fouling resistance for pristine membrane (PM), 760 °C coated membrane (LM), 860 °C coated membrane (HM) filtering 50 mg/L SA with 10 mM/L NaCl and 1 mM/L $CaCl_2$ at 90LMH.

Overall, the result showed that the presence of Ca^{2+} in low ionic strength (1mM) could decrease irreversible fouling and increase reversible fouling since the SA aggregates formed during complexation with Ca^{2+} would form a loose deposit on the membrane surface, resulting in irreversible fouling reduction (Lee et al., 2006). After adding NaCl (10 mM) and $CaCl_2$ (1 mM), TMP increased dramatically compared with the pure SA solution or SA solution adding calcium ions. Increased ionic strength by adding NaCl increases fouling rate because alginate and membrane charges are reduced through double layer compression and charge screening, resulting in decreased electrostatic repulsion between alginate molecules or between alginate and the membrane surface.

4.2.2 TOC Retention

As shown in Fig.23, two effects of fouling on rejection were observed. Firstly, the rejection of SA increased with the increase of filtration cycle in all experiments, most likely due to a reduction of pore size (pore constriction). Secondly, membrane fouling with organic matter generally increased the absolute value of the membrane's zeta potential, increasing the rejection rate of SA. Xu et al. has demonstrated similar findings (Xu et al., 2006).

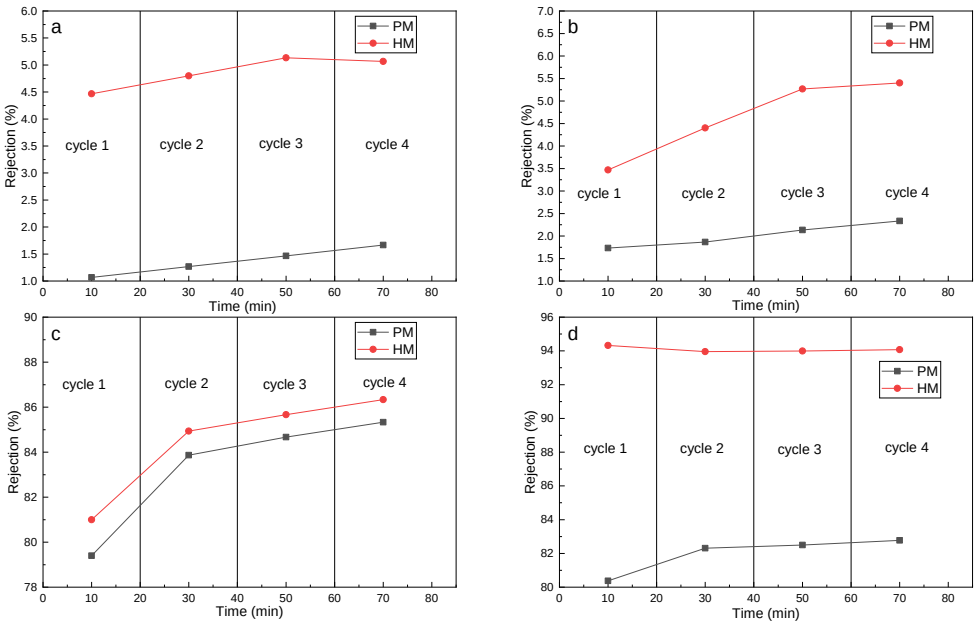

Fig. 23. TOC retention for pristine membrane (PM) and 860 ºC coated membrane (HM) at different conditions: (a) Flux = 80 LMH, 50 mg/L SA; (b) Flux = 90 LMH, 50 mg/L SA; (c) Flux = 90 LMH, 50 mg/L SA, 0.1 mM $CaCl_2$;(d) Flux = 90 LMH, 50 mg/L SA, 1 mM $CaCl_2$.

During the filtration experiments, when no Ca^{2+} was added to the feed solution, low rejection of the foulant is observed, as shown in Fig.23a and Fig.23b. The smaller SA molecular compared with membrane pore size could explain the low rejection rate of foulant. To improve the rejection rate, 1 mM Ca^{2+} was added, and 80% rejection was obtained for both pristine membrane (PM), and 860 ºC coated membrane (HM). But it was hard to distinguish the antifouling ability of PM and HM membranes until the concentration of Ca^{2+} was adjusted to 0.1 mM. This adjustment also improved the rejection rate from 4% to 80 %. Besides, a higher rejection rate led to an increase of TMP and total fouling resistance due to the formation of the cake layer, as shown in Fig 19, Fig 20, Fig 23c, Fig 23d. This behavior was consistent with prior research with MF membranes (Ye et al., 2005). Overall, for SA adding Ca^{2+}, the reversible fouling was dominant due to the formation of the cake layer, which could be largely removed with backwashing.

5. Conclusion

Colloidal fouling has attracted increasing interest, and O/W emulsion droplet and EPS are important colloids in produced water and surface water, respectively. There is an urgent demand to recycle oily wastewater since water scarcity is a huge change for undeveloped countries. Membrane technologies are a promising technology for recycling oil wastewater due to their smaller footprint and higher removal efficiency than conventional water treatment technologies (Hofs et al., 2011). Silicon carbide (SiC) ceramic membrane has advantages compared with other ceramic membranes, such as higher hydrophilicity and lower fouling tendency (Chen et al., 2020). Besides, the concept of threshold flux is essential and gives useful guidance in a practical situation and could provide a precise suggestion for the operator in the membrane-related industry (Field & Pearce, 2011).

The first objective is to determine the threshold flux of SiC MF membrane using O/W emulsions as model foulant. In this research, we monitored the real oily wastewater condition, and the effect of ionic strength, pH, surfactant concentration on threshold flux of 100 nm commercial SiC MF membrane produced by Liqtech company using an emulsion stabilized by the sodium dodecyl sulfonate (SDS) had been investigated. The results showed that for 25 cm SiC MF membrane, the threshold fluxes determined by the TMP_{avg} method when filtering 400 mg/L O/W emulsions with 100mg/L SDS, 400 mg/L SDS, 800 mg/L SDS, 10 mmol/L NaCl, 100 mmol/L NaCl were 108±6 LMH, 115±1 LMH, 129±5 LMH, 84 LMH, 67 LMH, respectively. Besides, the threshold fluxes determined by fouling rate method when filtering 400 mg/L O/W emulsions with 100mg/L SDS, 400 mg/L SDS, 800 mg/L SDS, 10 mmol/L NaCl, 100 mmol/L NaCl were 93±4 LMH, 110±14 LMH, 117±9 LMH, 64 LMH, 56 LMH, respectively. For 15 cm SiC MF membrane, the threshold fluxes determined by TMP_{avg} method when filtering 400 mg/L O/W emulsion with 100mg/L SDS, 400 mg/L SDS, pH =3, pH = 10, 10 mmol/L NaCl, 100 mmol/L NaCl were 96±1 LMH, 105 LMH, 84 LMH, 113 LMH, 76L LMH, 64 LMH respectively.

The membrane fouling leads to a severe decrease of permeability, resulting in a lower flux or higher TMPs, and zeta potential is an important property influencing fouling. Therefore, the second objective is to investigate the effect of SDS concentration, salinity, pH on zeta potential of O/W emulsion and fouling phenomenon of commercial SiC MF membrane. Overall, a more negatively charged surface group and the high absolute value of zeta potential could alleviate fouling. With an increase of SDS concentration, the absolute value of zeta potential increased until a certain value. With an increase of salt concentration from 0.01 M to 0.1 M, the mobility of particles decreased. The absolute value of zeta potential decreased from 90.8 mV to 68 mV since the positively charged Na^+ screened the charge of the negatively charged SDS head groups, reducing the electrostatic repulsion between the head groups and allowing more

surfactant molecules to adsorb. As a result, the interfacial tension decreased. However, the variation of pH did not influence the zeta potential of the O/W emulsion.

The DLVO theory has been illustrated in Section 2.4.2; According to this theory, a higher ionic strength could lead to a lower porosity of the cake layer and thus a higher TMP increase. With higher SDS concentration, the TMP increased more slowly due to higher membrane-droplet electrostatic repulsion. But there was no oil found in the permeate solution. The only contributing factor of the COD of permeate was the residual SDS. And this finding was confirmed by the data of COD of permeate. With an increase in salt concentration, the fouling would become much more severe. When salt concentration increased to 100 mM, the oil droplet penetrated the membrane and eventually went into permeate solution.

Moreover, SA has been chosen as a model foulant since it is commonly used as a substitute for EPS, which is the main organic pollutant in surface water (Katsoufidou et al., 2007). Therefore, the third objective is to assess the performance of SiC UF membranes and Al_2O_3 UF membranes using SA solution as model foulant in four-stage experiments and calculate the fouling resistance of membrane and obtain the retention of SA. For SA filtration, the effect of calcium ions and ion strength on membrane performances and fouling mechanisms of SiC UF membrane and Al_2O_3 UF membrane had been investigated. The result showed that the presence of Ca^{2+} in low ionic strength (1mM) could decrease irreversible fouling and increase reversible fouling since the SA aggregates formed during complexation with Ca^{2+} would deposit on the membrane surface and form a loose deposit, resulting in irreversible fouling reduction (Lee et al., 2006). After adding NaCl (10 mM) and $CaCl_2$ (1 mM), TMP increased dramatically compared with the pure SA solution or SA solution adding calcium ions. Increased ionic strength by adding NaCl increases fouling rate because alginate and membrane charges are reduced through double layer compression and charge screening, resulting in decreased electrostatic repulsion between alginate molecules or between alginate and the membrane surface. The SA rejection of the SiC-UF membrane increased with time during all the experiments. The rejection rate of SA increased with the increase of TMP. During the filtration experiments, when no Ca^{2+} was added to the feed solution, low rejection of the foulant was observed. To improve the rejection rate, 1 mM Ca^{2+} was added, and 80% rejection was obtained. But it was hard to distinguish between the pristine membrane and the 860 ^{o}C coated membrane. And the concentration of Ca^{2+} adjusted to 0.1 mM, which can not only distinguish pristine membrane and coated membrane but also improved the rejection rate. Overall, when fouling experiments operated with pure SA solution or SA solution with a low concentration of calcium ion, SiC UF membrane had a better anti-fouling ability compared with pristine Al_2O_3 UF membrane due to a lower reversible and irreversible fouling resistance and a slower increase of TMP.

6. Limitations and recommendations

Based on the design and results of the experiment, the following are some research suggestions for further research:

1. Commercial SiC MF membranes are not chemically stable. For 15 cm SiC MF membrane, the pure water permeance at 20^{o}C increases from 3000 $Lm^{-2}h^{-1}bar^{-1}$ to 4000 L $m^{-2}h^{-1}bar^{-1}$ after one month of use since the selective layer of membrane peeled off. For 15 cm SiC MF, a similar phenomenon occurred so that most experiments are performed only once.

2. It was reported that with an increase of SDS concentration, the droplet size distribution became narrow since an increase in SDS concentration led to relatively low interfacial tension by decreasing interfacial energy due to an increased surface area (Schroder and Schubert, 1998). But in this study, the conclusion contradicted it since high surfactant concentration led to larger droplets, and the mechanism could not be explained.

3. There are two different views on the effect of increasing concentration SDS on the negatively charged membrane. The first view showed that with higher SDS concentration, with the increase of the absolute value of zeta potential and the changes of membrane surface charge due to surfactant adsorption, the oil droplets and membrane surface are more negatively charged. The electrostatic repulsion between oil droplet and membrane surface enhanced, leading to a higher threshold flux (Mai et al., 2016). The second view is that SDS has a negative hydrophilic head group. SDS is absorbed on membrane surface at high SDS concentration by hydrophobic interaction, making membrane surface more hydrophobic and less negatively charged (Shi et al., 2019). At the same time, smaller oil droplets generated at high ionic strength, leading to standard pore blocking. As a result, with the increase of SDS concentration, the rejection rate decreases, and TMP increases because of the formation of the cake layer.

According to the analysis of permeate solution, only with high salinity (100mM), the penetration of oil into the membrane and eventually going into permeate solution occurred since it was beyond the critical pressure, which is the minimum pressure allowing oil droplet transport through the membrane. This critical pressure needs to be determined in future research by measuring oil-water interfacial tension since it can give some hints on when to stop experiments and clean the membrane.

7. Reference

Abro, D. M., Dablé, P., Cortés-Salazar, F., Amstutz, V., & Girault, H. (2016). Characterization of surface state of inert particles: case of Si and SiC. *Journal of Minerals and Materials Characterization and Engineering*, *4*(ARTICLE), 62-72.

Ahmad, T., Guria, C., & Mandal, A. (2020). A review of oily wastewater treatment using ultrafiltration membrane: A parametric study to enhance the membrane performance. *Journal of Water Process Engineering*, *36*, 101289.

Alresheedi, M. T., Basu, O. D., & Barbeau, B. (2019). Chemical cleaning of ceramic ultrafiltration membranes–Ozone versus conventional cleaning chemicals. *Chemosphere*, *226*, 668-677.

Ang, W. S., Lee, S., & Elimelech, M. (2006). Chemical and physical aspects of cleaning of organic-fouled reverse osmosis membranes. *Journal of membrane science*, *272*(1-2), 198-210.

Avranas, A., Stalidis, G., & Ritzoulis, G. (1988). Demulsification rate and zeta potential of O/W emulsions. *Colloid and Polymer Science*, *266*(10), 937-940.

Bacchin, P., Aimar, P., & Field, R. W. (2006). Critical and sustainable fluxes: theory, experiments and applications. *Journal of membrane science*, *281*(1-2), 42-69.

Bai, Z. S., Wang, H. L., & Tu, S. T. (2011). Oil–water separation using hydrocyclones enhanced by air bubbles. *Chemical Engineering Research and Design*, *89*(1), 55-59.

Beier, S. P., & Jonsson, G. (2010). Critical flux determination by flux-stepping. *AIChE journal*, *56*(7), 1739-1747.

Buffle, J., Wilkinson, K. J., Stoll, S., Filella, M., & Zhang, J. (1998). A generalized description of aquatic colloidal interactions: the three-colloidal component approach. *Environmental Science & Technology*, *32*(19), 2887-2899.

Cambiella, A., Benito, J. M., Pazos, C., & Coca, J. (2006). Centrifugal separation efficiency in the treatment of waste emulsified oils. *Chemical Engineering Research and Design*, *84*(1), 69-76.

Chen, V. (1998). Performance of partially permeable microfiltration membranes under low fouling conditions. *Journal of membrane science*, *147*(2), 265-278.

Choi, K. Y. J., & Dempsey, B. A. (2005). Bench-scale evaluation of critical flux and TMP in low-pressure membrane filtration. *Journal-American Water Works Association*, *97*(7), 134-143.

Cho, B. D., & Fane, A. G. (2002). Fouling transients in nominally sub-critical flux operation of a membrane bioreactor. *Journal of membrane science*, *209*(2), 391-403.

de Vos, W. M., & Lindhoud, S. (2019). Overcharging and charge inversion: Finding the correct explanation (s). *Advances in colloid and interface science*, *274*, 102040.

Derjaguin, B., & Landau, L. (1993). Theory of the stability of strongly charged lyophobic sols and of the adhesion of strongly charged particles in solutions of electrolytes. *Progress in Surface Science*, *43*(1-4), 30-59.

Dickhout, J. M., Virga, E., Lammertink, R. G., & de Vos, W. M. (2019). Surfactant specific ionic strength effects on membrane fouling during produced water treatment. Journal of colloid and interface science, 556, 12-23.

Dereli, R. K., Grelot, A., Heffernan, B., van der Zee, F. P., & van Lier, J. B. (2014). Implications of changes in solids retention time on long term evolution of sludge filterability in anaerobic membrane bioreactors treating high strength industrial wastewater. Water Research, 59, 11-22.

Elzo, D., Huisman, I., Middelink, E., & Gekas, V. (1998). Charge effects on inorganic membrane performance in a cross-flow microfiltration process. *Colloids and Surfaces A: Physicochemical and Engineering Aspects*, *138*(2-3), 145-159.

Fakhru'l-Razi, A., Pendashteh, A., Abdullah, L. C., Biak, D. R. A., Madaeni, S. S., & Abidin, Z. Z. (2009). Review of technologies for oil and gas produced water treatment. *Journal of hazardous materials*, *170*(2-3), 530-551.

Field, R. W., Wu, D., Howell, J. A., & Gupta, B. B. (1995). Critical flux concept for microfiltration fouling. *Journal of membrane science*, *100*(3), 259-272.

Field, R. W., & Pearce, G. K. (2011). Critical, sustainable and threshold fluxes for membrane filtration with water industry applications. *Advances in colloid and interface science*, *164*(1-2), 38-44.

Frens, G., & Overbeek, J. T. G. (1972). Repeptization and the theory of electrocratic colloids. *Journal of Colloid and Interface Science*, *38*(2), 376-387.

Gregory, J. (2005). *Particles in water: properties and processes*. CRC Press.

Jiao, D., & Sharma, M. M. (1994). Mechanism of cake buildup in crossflow filtration of colloidal suspensions. *Journal of Colloid and Interface Science*, *162*(2), 454-462.

Govedarica, D. D., Šećerov-Sokolović, R. M., Kiralj, A. I., Govedarica, O. M., Sokolović, D. S., & Hadnađev-Kostić, M. S. (2015). Separation of mineral oil droplets using polypropylene fibre bed coalescence. *Hemijska industrija*, *69*(4), 339-345.

Hamaker, H. C. (1937). The London—van der Waals attraction between spherical particles. *physica*, *4*(10), 1058-1072.

Hanafy, M., & Nabih, H. I. (2007). Treatment of oily wastewater using dissolved air flotation technique. *Energy Sources, Part A*, *29*(2), 143-159.

Hering, J. G., & Morel, F. M. (1988). Humic acid complexation of calcium and copper. *Environmental science & technology*, *22*(10), 1234-1237.

Ho, C. C., & Zydney, A. L. (2002). Transmembrane pressure profiles during constant flux microfiltration of bovine serum albumin. *Journal of Membrane Science*, *209*(2), 363-377.

He, Z., Miller, D. J., Kasemset, S., Paul, D. R., & Freeman, B. D. (2017). The effect of permeate flux on membrane fouling during microfiltration of oily water. *Journal of membrane science*, *525*, 25-34.

Hua, F. L., Tsang, Y. F., Wang, Y. J., Chan, S. Y., Chua, H., & Sin, S. N. (2007). Performance study of ceramic microfiltration membrane for oily wastewater treatment. *Chemical Engineering Journal*, *128*(2-3), 169-175.

Hong, S., & Elimelech, M. (1997). Chemical and physical aspects of natural organic matter (NOM) fouling of nanofiltration membranes. *Journal of membrane science*, *132*(2), 159-181.

Israelachvili, J. N. (1992). Intermolecular and Surface Forces (New York: Academic).
Katsoufidou, K., Yiantsios, S. G., & Karabelas, A. J. (2005). A study of ultrafiltration membrane fouling by humic acids and flux recovery by backwashing: experiments and modeling. *Journal of Membrane Science*, *266*(1-2), 40-50.
Katsoufidou, K., Yiantsios, S. G., & Karabelas, A. J. (2007). Experimental study of ultrafiltration membrane fouling by sodium alginate and flux recovery by backwashing. *Journal of Membrane Science*, *300*(1-2), 137-146.
Kundu, P., & Mishra, I. M. (2016). Treatment of surfactant-stabilized oily wastewater using coalescing bed of bagasse fly ash (BFA) as a low-cost filter medium: modelling and optimization of process parameters. *Desalination and Water Treatment*, *57*(42), 19713-19726.
Kovalsky, P., Bushell, G., & Waite, T. D. (2009). Prediction of transmembrane pressure build-up in constant flux microfiltration of compressible materials in the absence and presence of shear. *Journal of Membrane Science*, *344*(1-2), 204-210.
Luo, J., Morthensen, S. T., Meyer, A. S., & Pinelo, M. (2014). Filtration behavior of casein glycomacropeptide (CGMP) in an enzymatic membrane reactor: fouling control by membrane selection and threshold flux operation. *Journal of membrane Science*, *469*, 127-139.
Lee, S., Ang, W. S., & Elimelech, M. (2006). Fouling of reverse osmosis membranes by hydrophilic organic matter: implications for water reuse. *Desalination*, *187*(1-3), 313-321.
Lee, S., & Elimelech, M. (2007). Salt cleaning of organic-fouled reverse osmosis membranes. *Water research*, *41*(5), 1134-1142.
Le Clech, P., Jefferson, B., Chang, I. S., & Judd, S. J. (2003). Critical flux determination by the flux-step method in a submerged membrane bioreactor. *Journal of membrane science*, *227*(1-2), 81-93.
Li, S., Heijman, S. G. J., Verberk, J. Q. J. C., & van Dijk, J. C. (2010). Influence of Ca and Na ions in backwash water on ultrafiltration fouling control. *Desalination*, *250*(2), 861-864.
Li, J., McClements, D. J., & McLandsborough, L. A. (2001). Interaction between emulsion droplets and Escherichia coli cells. *Journal of food science*, *66*(4), 570-657.
López-Vazquez, C. M., & Fall, C. (2004). Improvement of a gravity oil separator using a designed experiment. *Water, Air, and Soil Pollution*, *157*(1), 33-52.
Lobo, A., Cambiella, Á., Benito, J. M., Pazos, C., & Coca, J. (2006). Ultrafiltration of oil-in-water emulsions with ceramic membranes: Influence of pH and crossflow velocity. *Journal of Membrane Science*, *278*(1-2), 328-334.
Mai, Z., Butin, V., Rakib, M., Zhu, H., Rabiller-Baudry, M., & Couallier, E. (2016). Influence of bulk concentration on the organisation of molecules at a membrane surface and flux decline during reverse osmosis of an anionic surfactant. *Journal of Membrane Science*, *499*, 257-268.
Marshall, A. D., Munro, P. A., & Tragardh, G. (1996). Design and development of a cross-flow membrane rig to compare constant pressure and constant flux operation in ultrafiltration and microfiltration. *Food and bioproducts processing: transactions of the Institution of Chemical Engineers, Part C*.
Motsa, M. M., Mamba, B. B., & Verliefde, A. R. (2015). Combined colloidal and organic fouling of FO membranes: the influence of foulant–foulant interactions and ionic strength. *Journal of Membrane Science*, *493*, 539-548.

Miller, D. J., Kasemset, S., Wang, L., Paul, D. R., & Freeman, B. D. (2014). Constant flux crossflow filtration evaluation of surface-modified fouling-resistant membranes. *Journal of Membrane Science*, *452*, 171-183.
Metsämuuronen, S., Howell, J., & Nyström, M. (2002). Critical flux in ultrafiltration of myoglobin and baker's yeast. *Journal of Membrane Science*, *196*(1), 13-25.
Nabi, N., Aimar, P., & Meireles, M. (2000). Ultrafiltration of an olive oil emulsion stabilized by an anionic surfactant. *Journal of Membrane Science*, *166*(2), 177-188.
Prathapan, R., Thapa, R., Garnier, G., & Tabor, R. F. (2016). Modulating the zeta potential of cellulose nanocrystals using salts and surfactants. *Colloids and Surfaces A: Physicochemical and Engineering Aspects*, *509*, 11-18.
Shang, R., Verliefde, A. R., Hu, J., Heijman, S. G., & Rietveld, L. C. (2014). The impact of EfOM, NOM and cations on phosphate rejection by tight ceramic ultrafiltration. *Separation and Purification Technology*, *132*, 289-294.
Shi, L., Lei, Y., Huang, J., Shi, Y., Yi, K., & Zhou, H. (2019). Ultrafiltration of oil-in-water emulsions using ceramic membrane: Roles played by stabilized surfactants. *Colloids and Surfaces A: Physicochemical and Engineering Aspects*, *583*, 123948.
Schröder, V., Behrend, O., & Schubert, H. (1998). Effect of dynamic interfacial tension on the emulsification process using microporous, ceramic membranes. *Journal of colloid and interface science*, *202*(2), 334-340.
Stoller, M., Bravi, M., & Chianese, A. (2013). Threshold flux measurements of a nanofiltration membrane module by critical flux data conversion. *Desalination*, *315*, 142-148.
Taha, T., & Cui, Z. F. (2002). CFD modelling of gas-sparged ultrafiltration in tubular membranes. *Journal of membrane science*, *210*(1), 13-27.
Tanudjaja, H. J., Tarabara, V. V., Fane, A. G., & Chew, J. W. (2017). Effect of cross-flow velocity, oil concentration and salinity on the critical flux of an oil-in-water emulsion in microfiltration. *Journal of Membrane Science*, *530*, 11-19.
Tang, C. Y., Chong, T. H., & Fane, A. G. (2011). Colloidal interactions and fouling of NF and RO membranes: a review. *Advances in colloid and interface science*, *164*(1-2), 126-143.
Tiller, C. L., & O'Melia, C. R. (1993). Natural organic matter and colloidal stability: Models and measurements. *Colloids and Surfaces A: Physicochemical and Engineering Aspects*, *73*, 89-102.
Vigneswaran, S., & Kwon, D. Y. (2015). Effect of ionic strength and permeate flux on membrane fouling: Analysis of forces acting on particle deposit and cake formation. *KSCE Journal of Civil Engineering*, *19*(6), 1604-1611.
Vácha, R., Rick, S. W., Jungwirth, P., de Beer, A. G., de Aguiar, H. B., Samson, J. S., & van den Brink, P., Zwijnenburg, A., Smith, G., Temmink, H., & van Loosdrecht, M. (2009). Effect of free calcium concentration and ionic strength on alginate fouling in cross-flow membrane filtration. *Journal of Membrane Science*, *345*(1-2), 207-216.
Xu, P., Drewes, J. E., Kim, T. U., Bellona, C., & Amy, G. (2006). Effect of membrane fouling on transport of organic contaminants in NF/RO membrane applications. *Journal of Membrane Science*, *279*(1-2), 165-175.

Xin, X., Zhang, H., Xu, G., Tan, Y., Zhang, J., & Lv, X. (2013). Influence of CTAB and SDS on the properties of oil-in-water nano-emulsion with paraffin and span 20/Tween 20. *Colloids and surfaces A: physicochemical and engineering aspects*, *418*, 60-67.
Ye, Y., Le Clech, P., Chen, V., & Fane, A. G. (2005). Evolution of fouling during crossflow filtration of model EPS solutions. *Journal of Membrane Science*, *264*(1-2), 190-199.
Ye, Y., Chen, V., & Fane, A. G. (2006). Modeling long-term subcritical filtration of model EPS solutions. *Desalination*, *191*(1-3), 318-327.
Zouboulis, A. I., & Avranas, A. (2000). Treatment of oil-in-water emulsions by coagulation and dissolved-air flotation. *Colloids and Surfaces A: Physicochemical and Engineering Aspects*, *172*(1-3), 153-161.

Appendix

A. Procedure for Particle size distribution (PSD)

Turn on the PC:

Username: TUD276989\localadmin

Password: Welkom04

Turn on both units:

Execute the Microtrac FLEX icon in the desktop.

Go to Measure □Open analyzer □Bluewave

Then click in the icon “SOP” and choose “Guangze”. Hit “Yes” and “Close”.

Hit the icon “AUTO” and wait until the window “Identifiers data entry” pops up.

Set sample name (e.g. 20210123) and click ok.

Mix the mixed liquor and add around 2mL (one Pasteur pipette) to the sampler and close it.

The device will automatically do the measurement in triplicates, and after around 5 minutes the sample will be finished.

B Characteristics of O/W emulsion

B.1 PSD results

(a)

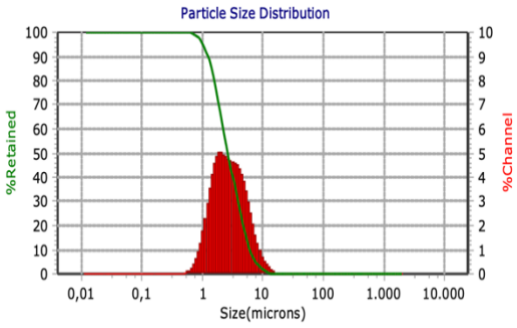

(b)

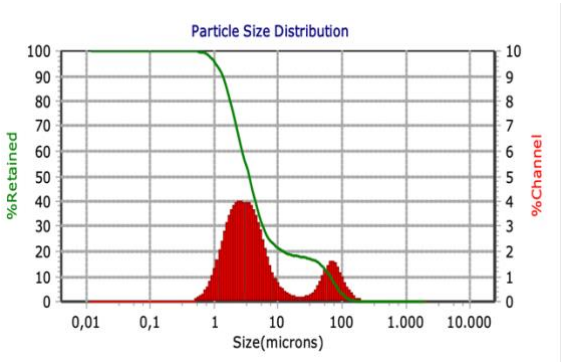

(c)

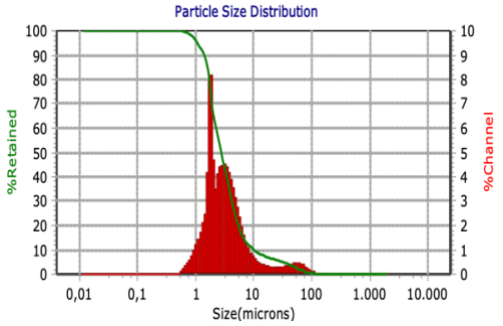

(d)

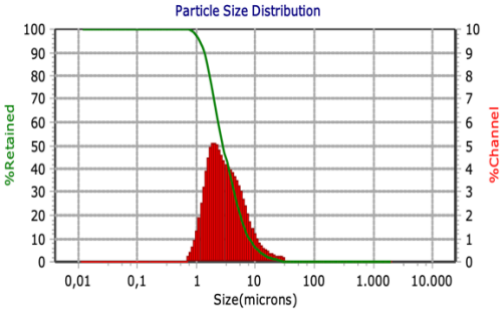

(e)

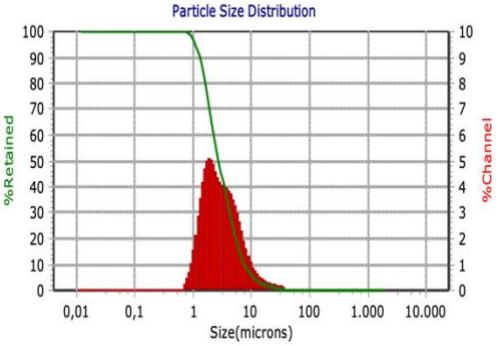

(f)

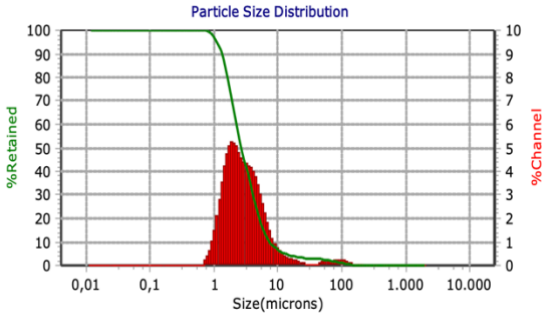

(g)

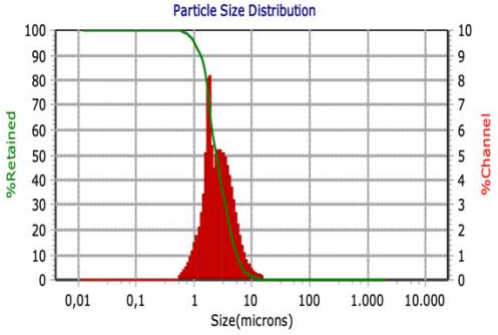

Fig.B.1. The particle size distribution under different conditions (a) 400 mg/L oil, 100 mg/L SDS; (b) 400 mg/L oil, 400 mg/L SDS; (c) 400 mg/L oil, 800 mg/L SDS; (d) 400 mg/L oil, 100 mg/L SDS, pH = 3; (e) 400 mg/L oil , 400 mg/L SDS, pH = 10; (f) 400 mg/L oil, 100 mg/L SDS, 10 mM NaCl; (g) 400 mg/L oil, 100 mg/L SDS, 100 mM NaCl.

B.2 Effect of standing time and dilution

(a)

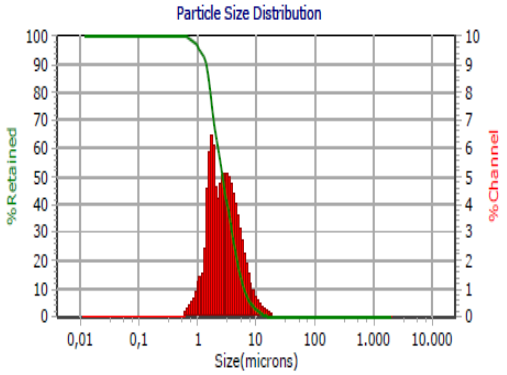

(b)

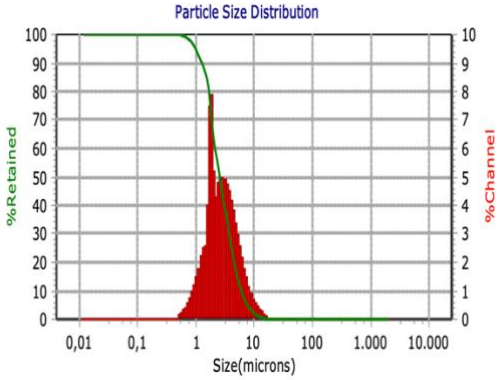

(c)

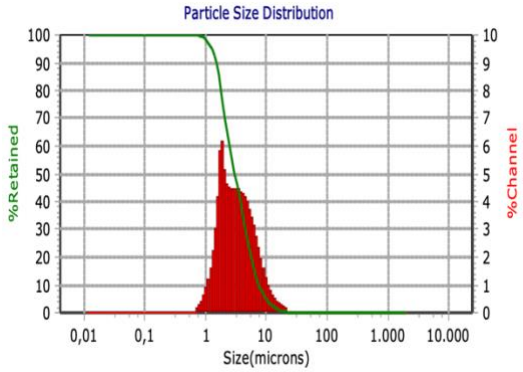

(d)

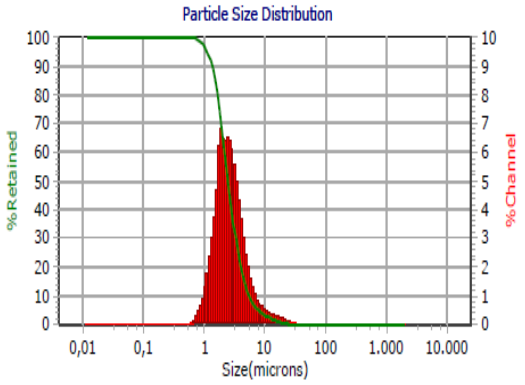

(e)

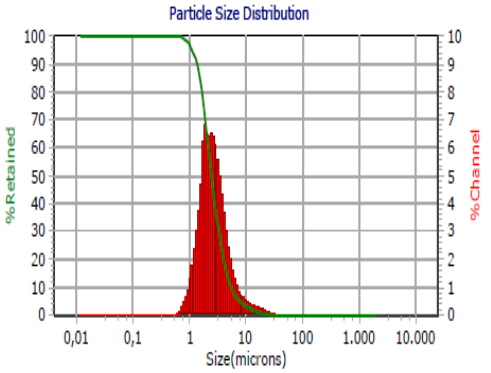

(f)

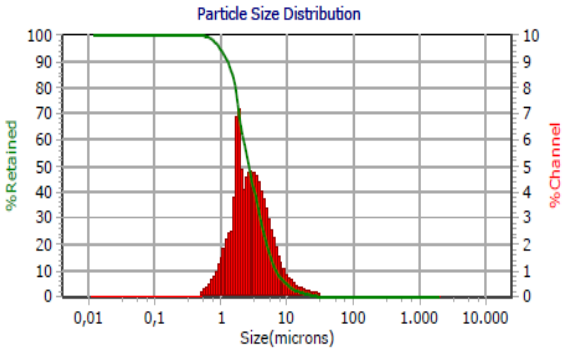

(g)

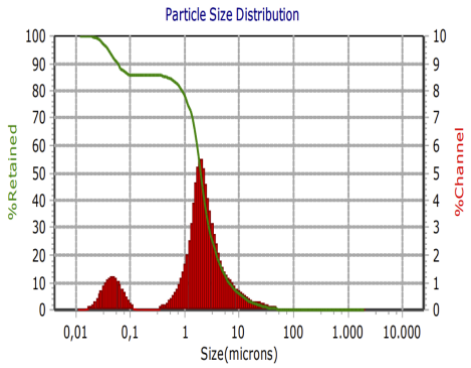

Fig.B.2. The particle size distribution under different conditions (a) Mix (24hr) + Sonication (40%/30min); (b) Mix (24hr) + Sonication (40%/30min) + standing time (12h); (c) Mix (24hr) + Sonication (40%/30min) + standing time (24h); (d) Mix (24hr) + Sonication (40%/30min) + standing time (24h) + Dilution(9x); (e) Mix (24hr) + Sonication (40%/30min) + standing time (24h) + Dilution(9x); (f) Mixing (48hr) + Sonication (40%/30min); (g) Mix (48hr) + Sonication (40%/30min) + standing time (24h) + Dilution (9x).

B.3 Zeta potential of O/W emulsion

Table B.1 The detailed data about zeta potential of O/W emulsion

Sample name	Zeta Potential 1 mV	Zeta Potential 2 mV	Average Zeta Potential mV	Standard Deviation mV	Conductivity mS/cm
1: 400mg/L oil + 100 mg/l SDS	-96.8 -96 -98.2	-81.9 -85.8 -89.3	-91.3	6.7	0.245
2: 400mg/L oil + 400 mg/l SDS	-104 -108 -109	-104 -105 -109	-106.5	2.4	0.425
3: 400mg/L oil + 800 mg/l SDS	-104 -105 -111	-104 -108 -110	-107	3.1	1.262
4: 400mg/L oil + 100 mg/l SDS + 10 mmol/L NaCl	-88.4 -90.4 -98.3	-85.2 -90.8 -91.6	-90.8	4.3	1.617
5: 400mg/L oil + 100 mg/l SDS +	-64.6 -68 -69.8	-65.2 -69.9 -70.1	-68.0	2.5	12.15

100 mmol/L NaCl					
6: 400mg/L oil + 100 mg/l SDS (PH = 3)	-81.2 -85.9 -90.7	-84.1 -87.2 -87.8	-86.2	3.3	0.305
7: 400mg/L oil + 100 mg/l SDS (PH = 10)	-81.7 -87.3 -86.5	-84.7 -87.2 -88.0	-85.9	2.3	0.255

B.4 absorbance spectroscopy

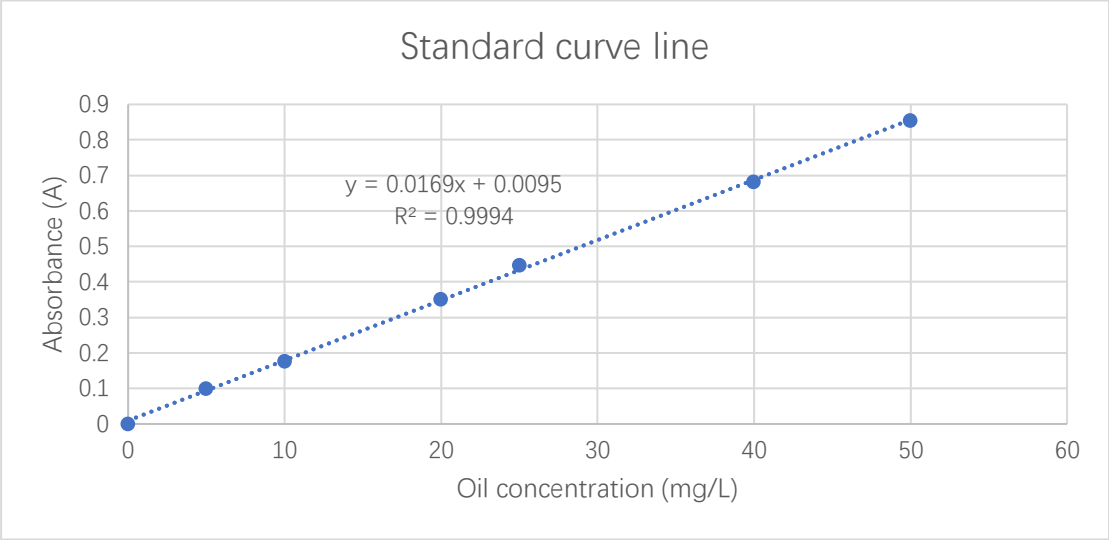

Fig.B.3. The relation between oil concentration and peak height in absorbance spectroscopy.

B.5 The amount of residue SDS in permeate under different flux

Table B.2 The amount of residue SDS in permeate under different flux

Flux (LMH)	100 mg/L SDS	400 mg/L SDS	800 mg/L SDS	pH = 3	pH = 10	10 mM NaCl
Unit	mg	mg	mg	mg	mg	mg
30	66.5	218.5	-	71.8	68.5	73.0
40	68.0	242.0	-	73.0	70.0	73.5
50	72.1	239.0	-	77.8	71.0	79.0
60	78.0	240.5	505.8	77.3	71.0	81.0
70	79.0	252.5	543.8	83.5	71.8	86.5
80	81.5	256.8	588.8	88.5	70.5	95.0
90	87.0	257.5	602.3	91.5	71.0	95.0

100	92.8	264.5	624.8	99.0	72.5	98.0
110	94.3	276.5	684.0	97.0	73.3	99.5
120	93.0	288.5	694.5	-	74.0	-
130	-	-	699.5	-	-	-
140	-	-	725.0	-	-	-
150	-	-	755.0	-	-	-

C Threshold flux

C.1 TMP_{avg} method for 25 cm SiC MF membrane

(a)

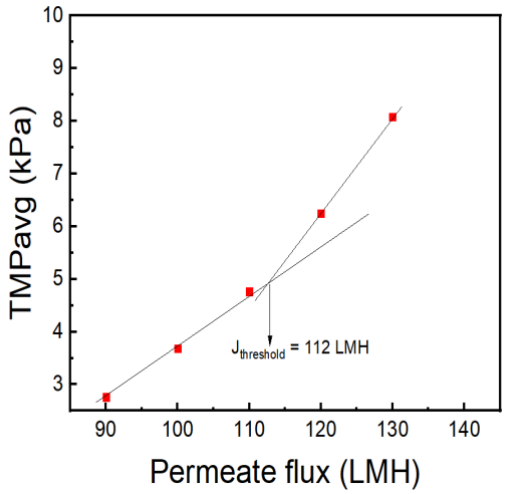

(b)

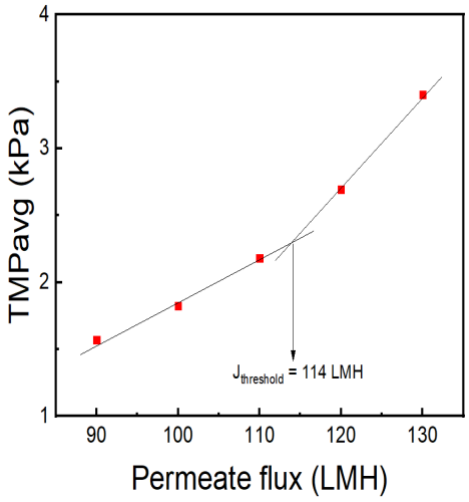

(c)

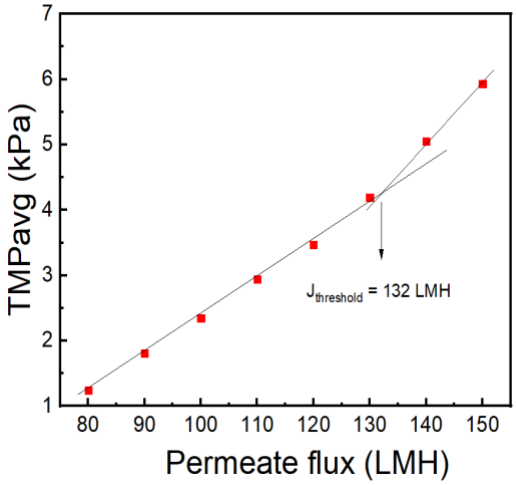

Fig. 24. The TMP_{avg} vs permeate flux for 25 cm SiC MF membrane filtering 400 mg/L oil and (a) 100 mg/L SDS; (b) 400 mg/L SDS; (c) 800 mg/L SDS.

C.2 Fouling rate method for 25 cm SiC MF membrane

(a)

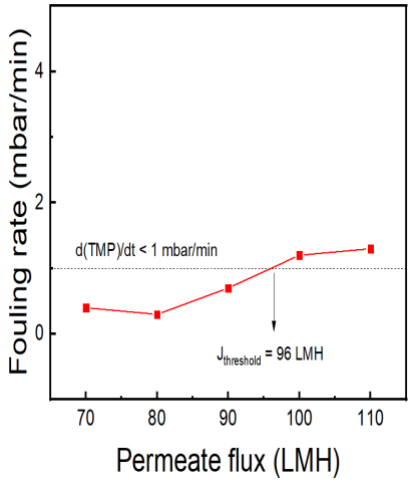

(b)

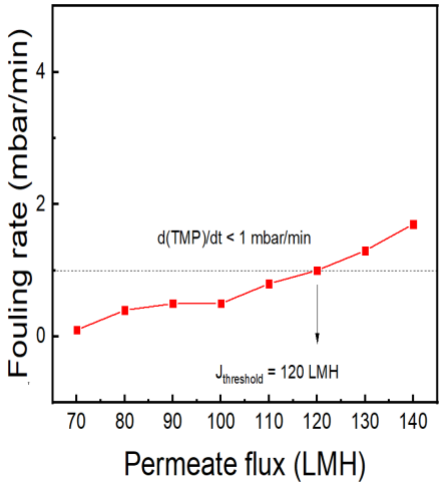

(c)

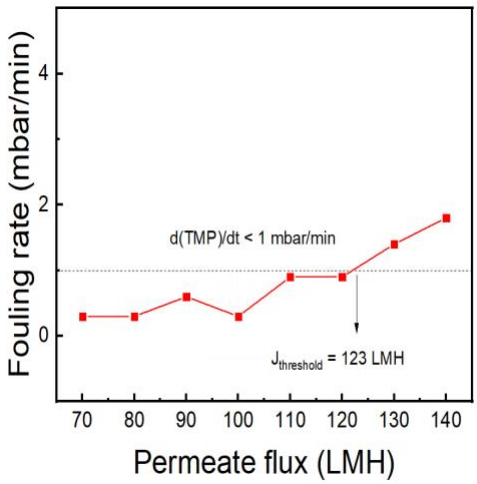

Fig. 25. The fouling rate vs permeate flux for 25 cm SiC MF membrane filtering 400 mg/L oil and (a) 100 mg/L SDS; (b) 400 mg/L oil, 400 mg/L SDS; (c) 400 mg/L oil, 800 mg/L SDS.

C.3 TMP_{avg} method for 15 cm SiC MF

(a)

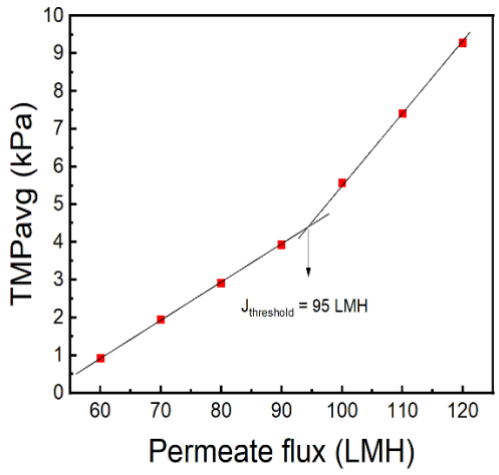

(b)

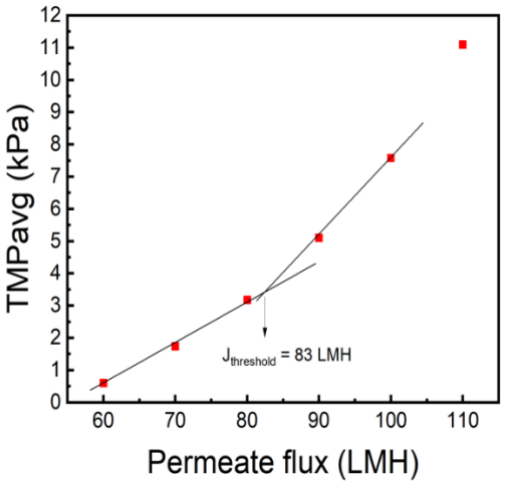

(b)

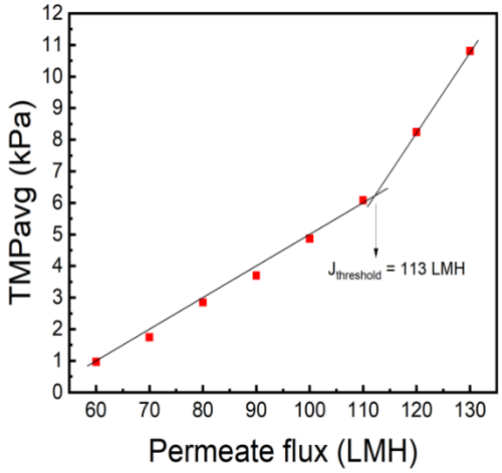

(d)

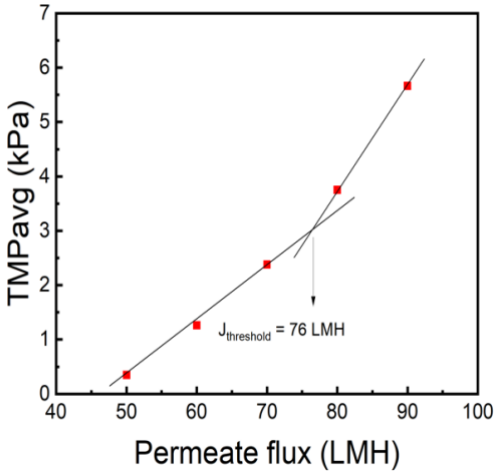

(e)

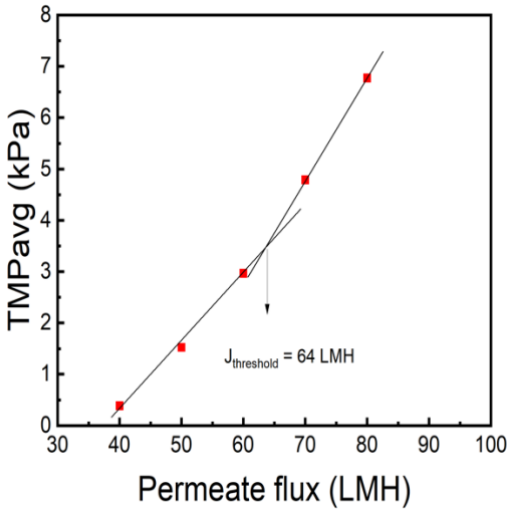

(f)

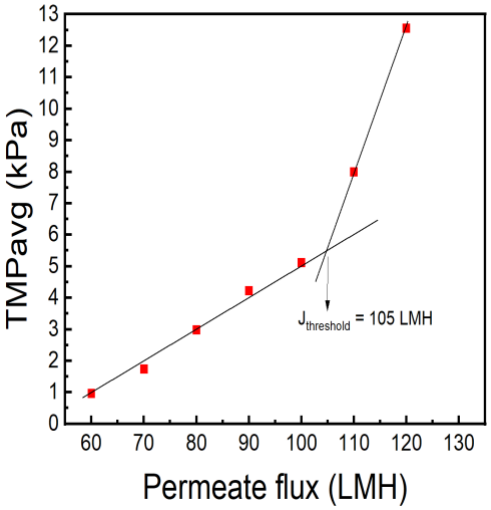

Fig. 26. The TMP_{avg} vs permeate flux for 25 cm SiC MF filtering 400 mg/L oil and (a) 100 mg/L SDS; (b) 100 mg/L SDS, pH = 3; (c) 100 mg/L SDS, pH = 10; (d) 100 mg/L SDS, NaCl = 10 mM; (e) 100 mg/L SDS, 100 mM NaCl; (f) 400 mg/L SDS.

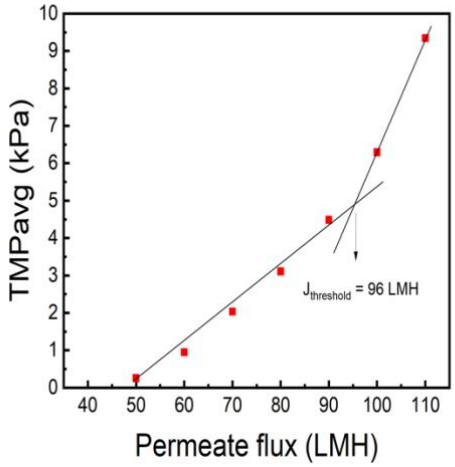

Fig. 27. The TMP_{avg} vs permeate flux for 15 cm SiC MF filtering 400 mg/L oil with 100 mg/L SDS

C.4 The summary of threshold flux for 15 cm and 25 cm SiC MF membrane

Table C.1. The summary of threshold flux for 15 cm and 25 cm SiC MF membrane.

Solution	TMP_{avg} method (25 cm SiC MF membrane)	d(TMP)/dt method (25 cm SiC MF membrane)	TMP_{avg} method (15 cm SiC MF membrane)
Unit	LMH	LMH	LMH
400 mg/L oil + 100 mg/L SDS	108±6	93±4	96±1
400 mg/L oil + 400 mg/L SDS	115±1	110±14	105
400 mg/L oil + 800 mg/L SDS	129±5	117±9	-
400 mg/L oil + 100 mg/L SDS + 10 mmol/L NaCl	84	64	84
400 mg/L oil + 100 mg/L SDS + 100 mmol/L NaCl	67	56	113
400 mg/L oil + 100 mg/L SDS (pH = 3)	-	-	76
400 mg/L oil + 100 mg/L SDS (pH = 10)	-	-	64